Extinction Map of the Galactic center: OGLE-II Galactic bulge fields

Takahiro Sumi

Princeton University Observatory, Princeton, NJ 08544-1001, USA, e-mail: sumi@astro.princeton.edu

Accepted Received in original form

ABSTRACT

We present the reddening (E(V-I)) and Extinction maps in V-band (A_V) and I-band (A_I) for 48 Optical Gravitational Lensing Experiment II (OGLE-II) Galactic bulge (GB) fields, covering a range of $-11^{\circ} < l < 11^{\circ}$, with the total area close to 11 square degrees. These measurements are based on two-band photometry of Red Clump Giant (RCG) stars in OGLE-II VI maps of GB. We confirm the anomalous value of the ratio of total to selective extinction $R_{VI} \equiv A_V/E(V-I) = 1.9 \sim 2.1$, depending on the line of sight, as measured by Udalski (2003). By using the average value of $R_{VI} = 1.964$ with the standard deviation sdev = 0.085, we measured E(V - I), A_V and A_I , and we obtained extinction and reddening maps with a high spatial resolution of 26.7" \sim 106.8", depending on the stellar density of each field. We assumed that average, reddening corrected colours of red clump giants are the same in every field. The maps cover the range 0.42 < E(V-I) < 3.5, $0.83 < A_V < 6.9$ and $0.41 < A_I < 3.4$ mag respectively. The zero points of these maps are calibrated by using V - K colours of 20 RR Lyrae ab variables (RRab) in Baade's window. The apparent reddening corrected I-band magnitudes of the RCGs change by +0.4 mag while the Galactic coordinate l varies from $+5^{\circ}$ to -5° , indicating that these stars are in the Galactic Bar. The reddening corrected colour of RRab and RCGs in GB are consistent with colours of local stars, while in the past these colours were claimed to

Key words: dust, extinction – Galaxy:bulge – Galaxy:center – stars:horizontal branch – stars:variables:other

1 INTRODUCTION

A study of stellar populations and stellar dynamics in the Galactic Bulge (GB) is important for understanding how bulges formed, what are their populations, gravitational potential and structure.

Several gravitational microlensing survey groups have found hundreds of events towards the Galactic center and disc (EROS: Derue 1999; OGLE: Udalski et al. 2000; Woźniak et al. 2001; MACHO: Alcock et al. 2000; MOA: Bond et al. 2001; Sumi et al. 2003a), and thousands are expected in the upcoming years by MOA ¹, OGLE-III ² and other collaborations. The data from such microlensing surveys is useful to study the Galactic structure by measuring the microlensing optical depth (Udalski et al. 1994; Alcock et al. 1997, 2000; Sumi et al. 2003a; Afonso et al. 2003; Popowski et al 2003;) and the proper motions of stars (Sumi, Eyer & Woźniak 2003; Sumi et al. 2003b), and well

suited for numerous other scientific projects (see Paczyński 1996; Gould 1996).

However, as is well known, the extinction due to the dust is very significant towards the GB. This affects the Color Magnitude Diagram (CMD) of the field and makes a separation of stellar populations difficult. To correct for these effects the measurements of the extinction in these fields are crucial.

Schlegel, Finkbeiner & Davis (1998) made all sky extinction map using COBE/DIRBE data, which overestimate the extinction towards the GB because of background dust (Dutra et al. 2003). Schultheis et al. (1999) and Dutra et al. (2003) constructed K-band extinction maps of the Galactic central region with a resolution of 4' by using J and K photometry of the upper giant branch stars in DENIS and 2MASS data respectively. Some determinations of the extinction towards Baade's Window have been performed with a number of different techniques, including those of stellar simulation (Ng et al. 1996), mean magnitudes of red-clump stars (Kiraga, Paczyński & Stanek 1997), the absolute magnitude of RR Lyrae stars (Alcock et al. 1998b) and magni-

¹ http://www.phys.canterbury.ac.nz/~physib/alert/alert.html

http://www.astrouw.edu.pl/~ogle/ogle3/ews/ews.html

tude of the K-giants (Gould, Popowski & Terndrup 1998). The Large-Scale Extinction Map of the Galactic Bulge was made by using the mean colour of all stars in the MACHO Project Photometry (Popowski, Cook & Becker 2003)

Woźniak & Stanek (1996) proposed a method to investigate the ratio of total to selective extinction based on two-band photometry of Red Clump Giants (RCGs). The RCGs are the equivalent of the horizontal branch stars for a metal-rich population, i.e., relatively low-mass core helium burning stars. RCGs in the Galactic bulge occupy a distinct region in the colour magnitude diagram (Stanek et al. 2000 and references therein). The intrinsic width of the luminosity and colour distribution of RCGs in the Galactic bulge is small, about 0.2 mag (Stanek et al. 1997; Paczyński & Stanek 1998).

The CMD is used to obtain the quantitative values of the offset on the CMD between the different subfields, caused by differential extinction. They used RCGdominated parts of the CMDs for determining the offsets, the clump being seen at fainter magnitudes and redder colours in subfields with higher extinction. They applied this method to the OGLE-I data and then found the ratio of total to selective extinction $R_{VI} \equiv A_V/E(V-I) = 2.44$. This is consistent with Ng et al. (1996). Stanek (1996) applied this method to the OGLE-I data to obtain differential extinction A_V and reddening E(V-I) in a $40' \times 40'$ region of Baade's window, with resolution of $\sim 30''$. They estimated $R_{VI} = 2.49 \pm 0.02$. Paczyński et al. (1999) and Sumi et al. 2003a applied this method to OGLE-II ($14'.2 \times 14'.2$ with resolution of $20'' \times 20''$) and MOA (16 deg² with resolution of $3.45' \times 3.45'$) data respectively. They first made a reddening map for their fields because determining the reddening E(V-I) (horizontal shift in the CMD) is easier than A_V and A_I (vertical shift in the CMD). Then the extinction map was calculated according to the following formulae:

$$A_I = R_I \times E(V - I), \tag{1}$$

$$A_V = R_{VI} \times E(V - I). \tag{2}$$

with "standard" values of $R_{VI}=2.5$ and $R_{I}\equiv A_{I}/E(V-I)=1.5$.

Paczyński & Stanek (1998) and Stutz, Popowski & Gould (1999) found that the mean V-I colours of GB RCGs and RR Lyrae, dereddened with Stanek's map, are redder than colours of their nearby counterparts. Popowski (2000) summarized possible explanations of these discrepancies, and noted that the simplest and the most plausible explanation is a non-standard interstellar extinction. The discrepancy would vanish if $R_{VI}=2.1$ rather than the standard value of 2.5. Udalski (2003) showed that there is indeed an anomaly in the extinction law, with $R_{VI}=1.9\sim2.3$, depending on the direction of the line of sight.

In this paper we confirm the anomalous value of R_{VI} , and by using new value, we construct extinction maps for 48 Galactic Bulge fields observed by the Optical Gravitational Experiment ³ II (OGLE-II; Udalski et al. 2000).

In § 2 we describe the data. We measure the reddening

see http://www.astrouw.edu.pl/~ogle or

http://bulge.princeton.edu/~ogle

line in \S 3. We construct the reddening and extinction maps in \S 4. Discussion and conclusion are given in \S 5.

2 DATA

We use the VI photometric maps of standard OGLE template (Udalski et al. 2002), which contain VI photometry and astrometry of ~ 30 million stars in the 49 GB fields. Positions of these fields (BUL-SC1 \sim 49) can be seen in Udalski et al. (2002). We do not use BUL_SC44 in this work because most of RCGs in this field are close to, or even below the V-band detection limit of OGLE due to high extinction. The photometry is the mean photometry from a few hundred measurements in the I-band and several measurements in V-band collected during the second phase of the OGLE experiment between 1997 and 2000. Accuracy of the zero points of photometry is about 0.04 mag. A single 2048 × 8192 pixel frame covers an area of $0.24 \times 0.95 \text{ deg}^2$ with pixel size of 0.417 arcsec/pixel. Details of the instrumentation setup can be found in Udalski, Kubiak & Szymański (1997).

3 THE RATIO OF TOTAL TO SELECTIVE EXTINCTION

To measure the ratio of total to selective extinction, i.e. $R_I \equiv A_I/E(V-I)$, we make use of the position of RCGs in the (I, V - I) CMD, as it was done by Udalski (2003), but contrary to Woźniak & Stanek (1996) and Stanek (1996), who used the (V, V - I) CMD. The reddening corrected Iband magnitude of the RCGs does not vary with colour, while the V-band magnitude is a function of V-I(Paczyński & Stanek 1998), and using it can lead to systematic errors (Popowski 2000). We make a preliminary assumption that the average, reddening corrected RCG colour is constant, $\langle V - I \rangle_{0,RC} = 1.0$, which is approximately the colour of nearby RCGs as measured by Hipparcos (Paczyński & Stanek 1998). The mean colour $\langle V-I \rangle_{\rm RC}$ and I-band magnitude $\langle I \rangle_{\rm RC}$ of RCGs follow reddening line with a slope R_I and a constant $I_{0,RC}$, to be determined for every field

$$\langle I \rangle_{RC} = I_{0,RC} + R_I (\langle V - I \rangle_{RC} - \langle V - I \rangle_{0,RC}). \tag{3}$$

In this Section, we measure the slope R_I and brightness of RCGs $I_{0,RC}$ in Eq.3, with a low spacial resolution, but with a significant number of RCGs. In the next Section, we measure the colour of RCGs with high spacial resolution by using these R_I and $I_{0,RC}$. This is because an identification of RCG centroids in I is more difficult than in V-I because of the vertical structure of Red Giants overlapping RCGs in the CMD.

In this Section, there are 2 steps to find the RCG centroids in the CMD. At a first step, we divide the field into "bins" to take spacial differences of the extinctions into account, then we measure the rough mean colour of RCGs in each bin. At a second step, we combine bins with similar RCG colour into group to enlarge the significance of RCGs, then we estimate the RCG centroids by the Gaussian fit.

As a first step, we divide each field into $16 \times 64 = 512$ "bins" which have 128×128 pixels each. As these "bins" are

relatively large there may be a considerable differential reddening within them, and the RCG may be elongated along the reddening line.

We select an elongated window within which the RCGs are located, following the reddening line as given by the Eq. (3) with a width of ± 0.5 mag in I. As we do not know the correct reddening slope and the correct magnitude of RCGs, we adopt a broad range of trial values: $0.6 < R_I < 2.0,$ and $14 < I_{0,RC} < 15.$ We also adopt a broad range of colours for the search of RCGs, selected to be within 1.4 < (V-I) < 5; the boundaries are adjusted for each field to minimize the contamination by blue disk main sequence stars and faint red bulge main sequence stars. We measure the average $\langle V-I\rangle_{\rm RC}$ in each bin using 2- σ clipping. These values are used as the initial values of the RCGs colour in the next paragraph.

In a given bin we measure the average colour and magnitude of RCGs within the circle with a radius of 0.4 mag in the CMD centered at the colour $\langle V-I\rangle_{\rm RC}$ on the reddening line. These new average values: $\langle V-I\rangle_{\rm RC}$ and $\langle I\rangle_{\rm RC}$, calculated for all 128×128 pixel bins, are used to obtain an improved value of R_I and $I_{0,RC}$. This process is iterated until the values of R_I and $I_{0,RC}$ do not change any more. We found that this final value for a given OGLE field was independent of the first guess in the ranges $0.6 < R_I < 2.0$ and $14 < I_{0,RC} < 15$, and are roughly the same as the more precise values measured in the second step.

Even if we locate the window slightly higher or lower, i.e. $I_{0,\mathrm{RC}}$ in Eq.(3), than the true RCG centroid in I, we would get roughly same colour as the true RCGs colour because the RCGs colour are very similar to the colours of red giants which are somewhat brighter or fainter than RCGs. We use only resultant average colour $\langle V-I\rangle_{\mathrm{RC}}$ of each bin in the following analysis, to arrange bins in order of their extinction in a given field. So, as long as we fix the value of R_I and $I_{0,RC}$ in a given field these colours can be used to arrange the bins.

As a second step we arrange the bins in a given field in order of extinction by using $\langle V-I\rangle_{\rm RC}$. Then we combined these bins into groups from low extinction to high extinction until each group is filled by ~ 1000 RCGs. Given a large number of RCGs in each group of bins we could find the RCGs positions in the CMD for each group independently. We measured RCGs centroid of each group in the CMD by following three methods:

[1] In a given group of bins we measure the average colour and magnitude of RCGs within the circle with a radius of 0.3 mag in the CMD, centered at the initial values of colour and magnitude of RCGs. These new average values are used for new RCG selection. This process is iterated until the value $\langle V-I\rangle_{\rm RC}$ and $\langle I\rangle_{\rm RC}$ do not change any more. We found these final values do not depend on their initial values which can be given by the rough positions of RCGs in previous section, as long as their real positions are within this initial circle.

[2] Similar with [1] but with a larger radius of 0.45 mag and weighting V-I and I with two dimensional Gaussian with $\sigma=0.15$ mag.

[3] We fit the distribution of stars in each group with the power law plus Gaussian luminosity function:

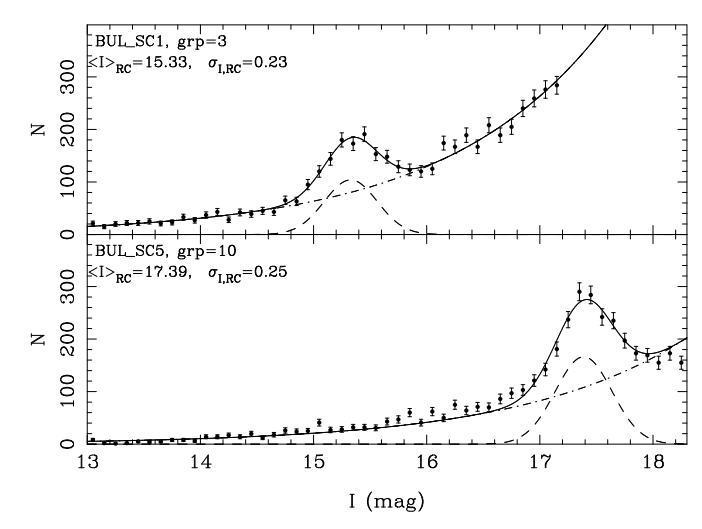


Figure 1. Sample *I*-band Luminosity Functions of stars in relatively low (upper panel: BUL_SC1, grp=3) and high (lower panel: BUL_SC5, grp=10) extinction fields. Solid lines are the best fits by equation (4). Dashed and dot-dashed lines represent the Gaussian and power law components in the best fits.

$$\phi_I(I) = p_0 10^{p_1 I} + p_2 \exp\left(-\frac{(I - \langle I \rangle_{RC})^2}{2\sigma_{I,RC}^2}\right),$$
 (4)

where p_0 , p_1 , p_2 and $\sigma_{I,RC}$ are free parameters, calculated for each group of bins separately. RCGs are selected within the circle with radius of 0.4 mag centered at this best fit $\langle I \rangle_{RC}$ and $\langle V - I \rangle_{RC}$ measured by method [1]. We fitted the colour distribution of selected RCGs with another Gaussian:

$$\phi_{VI}(V-I) = p_3 \exp\left(-\frac{((V-I) - \langle V-I \rangle_{\rm RC})^2}{2\sigma_{VI,\rm RC}^2}\right), \quad (5)$$

where p_3 and $\sigma_{VI,RC}$ are free parameters.

In Fig. 1 we show the sample *I*-band Luminosity Functions of stars in a relatively low (upper panel: BUL_SC1, grp=3) and high (lower panel: BUL_SC5, grp=10) extinction fields with the best fit by equation (4). Here groups (grp) which have roughly 1,000 RCGs are numbered from 1 in order of increasing extinction. One can see how significantly we can measure the RCGs centroids in these large groups.

We arrange 44 OGLE-II fields into 11 regions of fields close to each other, as presented in table 1. Regions A, B, C and D are identical with those in Udalski (2003). Fields BUL_SC6, 7, 47, 48, 49 are not analyzed because there are too few RCGs in these fields and very little differential extinction. We assume that the slope of the reddening line, R_I , is the same within each region, but it may be different in different regions. For every region we had a collection of groups of bins, and the values of centroids of the RCGs: $(\langle I \rangle_{RC}, \langle V - I \rangle_{RC})$ for each group. We fitted these data with Eq.(3). All R_I measured by different methods are consistent with each other within their errors. In the following analysis we use the results by method [3] because they have the smallest scatter in the fitting.

In Fig. 2 we show the distribution of centroids for regions (A), (B), (C) and (D) with the best fit lines. The best fit value R_I , the error σ , and the standard deviation sdev for all regions, and their average values are given in table

4 T. Sumi

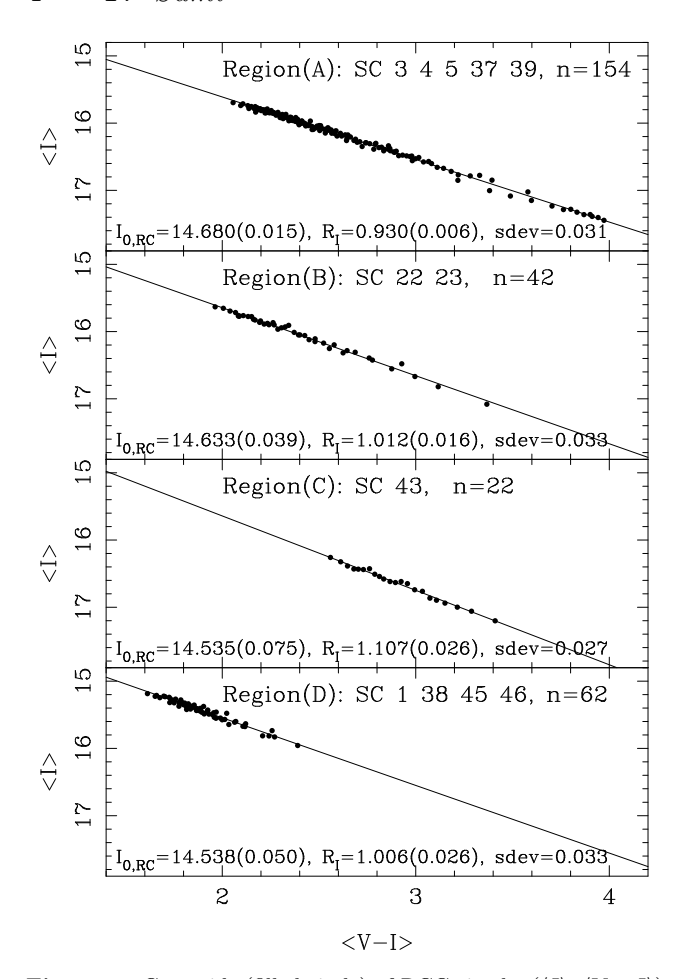


Figure 2. Centroids (filled circle) of RCGs in the $(\langle I \rangle, \langle V - I \rangle)$ CMD in the region (A), (B), (C) and (D) (from top to bottom) measured with method [3], as described in the text. The best fit line, parameters and the standard deviation (sdev) are also given in the figure.

1. We also give the the mean R_I for all regions except (A), because region (A) has a significantly smaller R_I than other fields, and it has a very small error. In region (A) (Top panel of Fig. 2), we did not use groups with $\langle V-I\rangle_{\rm RC}>4$ because they are close to detection limit in V-band, and their center in the CMD is shifted systematically to brighter I. We believe that groups with $\langle V-I\rangle_{\rm RC}<4$ are not affected by this effect because R_I does not change when this limit is reduced to smaller values.

Our values of R_I are consistent with Udalski (2003) and are significantly smaller than the standard reddening law (~ 1.5). The measured R_I are shown as a function of the Galactic longitude (l) and latitude (b) in Fig. 3. We can see that R_I is slightly different from region to region, but there is no strong systematic dependence on the Galactic coordinates l or b. There might be a weak dependence in l, $dR_I/dl = -0.0102 \pm 0.0049$. This trend gives the largest difference in R_I of 0.08 in regions (H) and (J). We think that this trend can be neglected in the following analysis because we take the scatter of 0.085 in R_I into account during the error estimation in reddening and extinctions.

In the following analysis we use the mean value of the reddening slope for all regions i.e. $R_I = 0.964$ with sdev = 0.085. The values of $I_{0,\rm RC}$, obtained by fitting Eq. (3) with

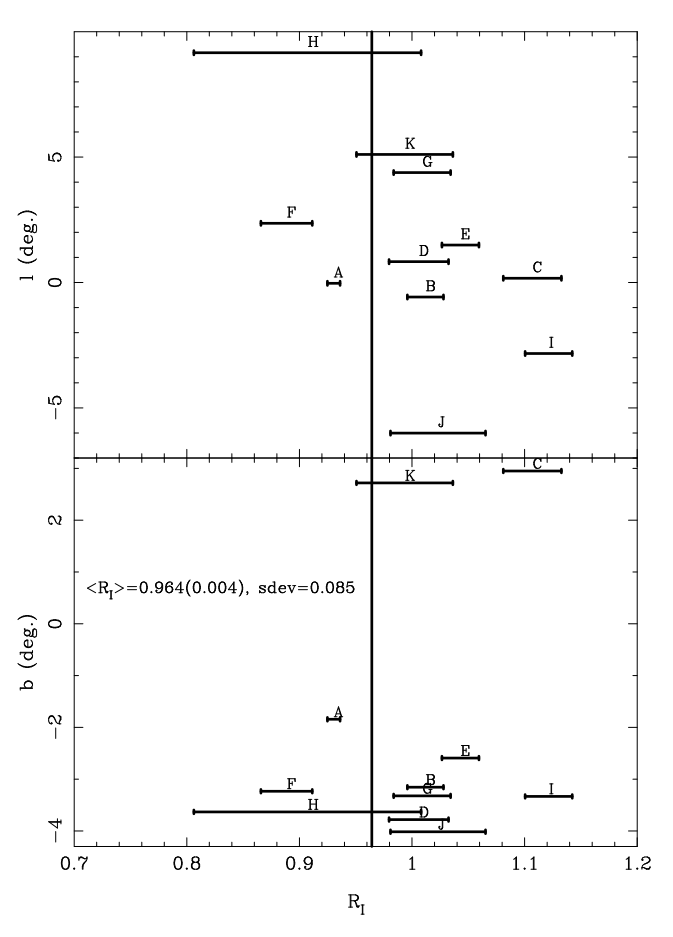


Figure 3. The ratio of total to selective extinction $R_I \equiv A_I/E(V-I)$ for each region as a function of Galactic coordinates. The values of R_I correspond to the middle of the error bars, and the average $\langle R_I \rangle$ is shown with a vertical line.

Table 2. Extinction corrected I magnitude of RCGs $I_{0,RC}$ measured with fixing $R_I = 0.964$ for each region.

| Region | $I_{0,RC}$ | $\sigma_{I_{0,RC}}$ | sdev | $I_{0,RC}^{\ast}$ | $\sigma_{I_{0,RC}^*}$ |
|--------------|------------|---------------------|-------|-------------------|-----------------------|
| A | 14.625 | 0.003 | 0.034 | 14.652 | 0.024 |
| В | 14.700 | 0.005 | 0.036 | 14.728 | 0.024 |
| C | 14.808 | 0.009 | 0.042 | 14.835 | 0.025 |
| D | 14.576 | 0.004 | 0.034 | 14.603 | 0.024 |
| \mathbf{E} | 14.551 | 0.003 | 0.031 | 14.578 | 0.024 |
| \mathbf{F} | 14.491 | 0.003 | 0.028 | 14.518 | 0.024 |
| G | 14.453 | 0.004 | 0.033 | 14.480 | 0.024 |
| H | 14.371 | 0.016 | 0.077 | 14.398 | 0.028 |
| I | 14.808 | 0.005 | 0.041 | 14.836 | 0.024 |
| J | 14.772 | 0.006 | 0.036 | 14.799 | 0.024 |
| K | 14.529 | 0.005 | 0.026 | 14.557 | 0.024 |

Note: $I_{0,RC}^*$ represent the value after the zero-point correction.

the fixed slope $R_I = 0.964$ for each region, are given in table 2 and are plotted in Fig. 4 as a function of Galactic coordinates l and b. A clear evidence of the bar is apparent between -4 < l < 4 in the upper panel of this figure, which is consistent with Stanek et al. (1997). Note that regions (C) and (K) are shifted with respect to the pattern indicated by regions (G), (F), (E), (D), (A), (B); they are on the other side of the Galactic plane, i.e. in b > 0.

| Region | fields (BUL_SC) | l(deg.) | b(deg.) | R_I | σ_{R_I} | sdev |
|-----------------|-------------------------|---------|---------|-------|----------------|-------|
| A | 3 4 5 37 39 | 0.168 | -1.844 | 0.930 | 0.006 | 0.031 |
| В | 22 23 | -0.380 | -3.155 | 1.012 | 0.016 | 0.033 |
| $^{\mathrm{C}}$ | 43 | 0.370 | 2.950 | 1.107 | 0.026 | 0.027 |
| D | 1 38 45 46 | 1.030 | -3.780 | 1.006 | 0.026 | 0.033 |
| \mathbf{E} | 20 21 30 34 | 1.692 | -2.593 | 1.043 | 0.016 | 0.028 |
| \mathbf{F} | $2\ 31\ 32\ 33\ 35\ 36$ | 2.560 | -3.233 | 0.889 | 0.023 | 0.027 |
| G | $16\ 17\ 18\ 19\ 42$ | 4.582 | -3.322 | 1.009 | 0.025 | 0.032 |
| Н | 8 9 10 11 12 13 | 9.360 | -3.632 | 0.907 | 0.101 | 0.078 |
| I | $24\ 25\ 40\ 41$ | -2.632 | -3.333 | 1.121 | 0.021 | 0.031 |
| J | 26 27 28 29 | -5.805 | -4.015 | 1.023 | 0.042 | 0.036 |
| K | 14 15 | 5.305 | 2.720 | 0.994 | 0.043 | 0.026 |
| All | - | - | - | 0.964 | 0.004 | 0.085 |
| without A | - | - | - | 1.026 | 0.008 | 0.075 |

Table 1. The ratio of total to selective extinction R_I for each region.

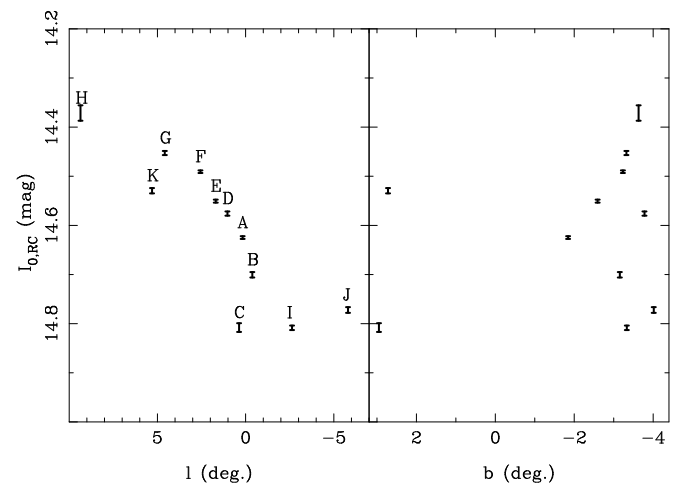


Figure 4. The constant $I_{0,\mathrm{RC}}$ (cf. Eq. (3)) is shown for each region as a function of Galactic coordinates adopting a fixed value $R_I=0.964$. The values correspond to the middle of error bars. Note region (C) and (K) are fields with b>0.

4 EXTINCTION MAP

4.1 Relative Reddening

In this section we estimate the mean RCGs colours for each bin $\langle V - I \rangle_{\rm RC}$, and we transform them to the relative reddening, $E(V-I)_{\rm RC} = \langle V-I \rangle_{\rm RC} - \langle V-I \rangle_{\rm 0,RC}$, assuming the intrinsic colour of RCGs $\langle V-I \rangle_{\rm 0,RC} = 1.0$. Then we estimate the relative extinctions in V-band $(A_{V,\rm RC})$ and I-band $(A_{I,\rm RC})$ by Eq. (2) and (1).

In the following analysis we adopt the reddening line with the slope $R_I=0.964$ and a constant $I_{0,RC}$ as given in table 2. Thanks to fixing R_I and $I_{0,RC}$, we can get accurate $\langle V-I\rangle_{\rm RC}$ with a smaller number of RCGs, i.e. with high resolution in space (small bin) and in reddening (small group). Furthermore we introduce a new indicator $\langle V-I\rangle_{\rm all}$ which is the average colour of all stars in each bin, to represents the level of extinction in each bin to arrange bins into group. Because the number of all stars are much larger than RCGs, we to get higher spacial resolution.

We divide each field into a new set of small "bins" with the size in the range 64×64 to 157×157 pixels, chosen so

that each bin has ~ 200 stars. Next, we measure the average colour of all stars in each bin, $(V - I)_{all}$. We also measure the average colour of RCGs in each "bin", $\langle V-I \rangle_{\rm RC}$, following method [1] described in the previous section, with a radius of 0.5 mag, allowing the center of RCGs to lie only on the reddening line. The initial values of $\langle V - I \rangle_{\rm RC}$ for this method are estimated by using the parallelogram along this reddening line. This may be fairly uncertain statistically as there are only several RCGs per bin, but may suffer from less systematics than $(V - I)_{all}$. We compare the two sets of colours in Fig. 6 (upper sequence) for the field BUL_SC22. There is good correlation between $\langle V - I \rangle_{\rm RC}$ and $\langle V - I \rangle_{\text{all}}$. Other fields have similar trends, but the slops are not always 1. This good correlation imply that $\langle V - I \rangle_{\rm all}$ can be a good extinction indicator, as suggested by Popowski, Cook & Becker (2003).

We arrange bins in a given field in order of extinction by using $\langle V-I\rangle_{\rm all}$. Then we combine these bins into groups from low extinction to high extinction until each group is filled by ~ 100 RCGs. Note that groups in § 3 have $\sim 1,000$ RCGs.

In Fig. 5 we show an example of a CMD for two groups of bins in BUL_SC22, one with low extinction (filled circles) and one with high extinction (open circles). We calculate the average colour of RCGs $\langle V-I\rangle_{\rm RC,g}$ for each group of bins using the method described in previous paragraph. As described above, thanks to fixing R_I and $I_{0,RC}$, we can get accurate $\langle V-I\rangle_{\rm RC,g}$ because the RCGs colour are very similar to the colours of red giants which are somewhat brighter or fainter than RCGs.

There is a very good correlation between these colours and $\langle V-I\rangle_{\rm RC}$ obtained for single bins, as shown in Fig. 6 (lower sequence). In this figure the typical width of $\langle V-I\rangle_{\rm RC}$ of bins in each group can be seen by the gaps of $\langle V-I\rangle_{\rm RC,g}$, about < 0.1 mag depending on the number density of stars. We adopt $\langle V-I\rangle_{\rm RC,g}$ as the mean colour of RCGs for bins in this group, because these are based on the large statistics of RCGs.

Some bins were not included in any group for variety of reasons: (1) a bin has fewer than 20 stars, (2) a bin has a very bright blue star (mimics low extinction), (3) a bin has a very bright red star (mimics high extinction). (4) because of a very high extinction a large fraction of Bulge red giants is below the detection limit, so these bins can not be grouped

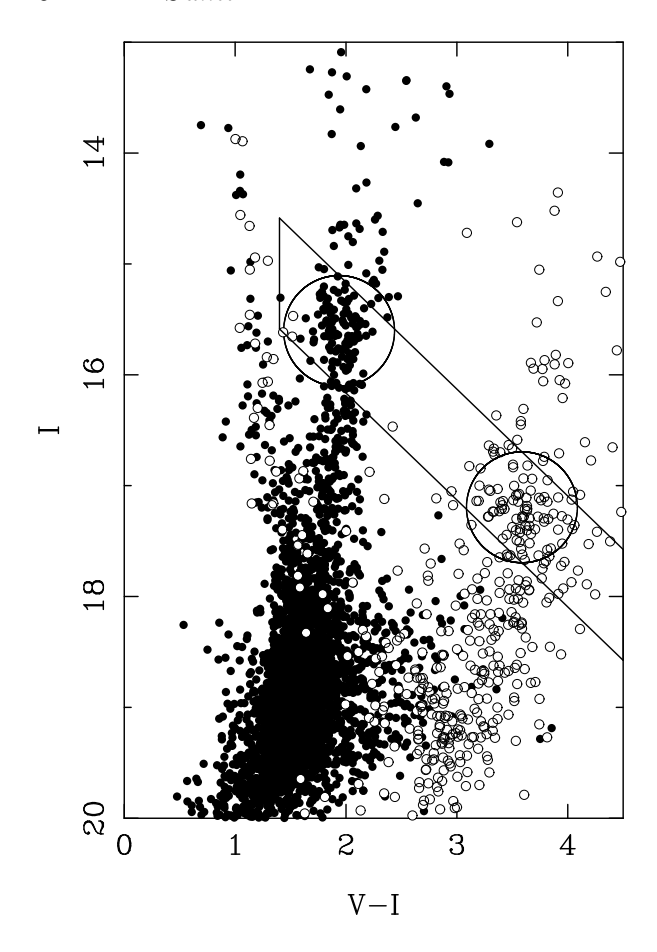


Figure 5. The CMDs of two groups in BUL_SC22. Filled and open circles represent stars in a group with low and high extinction, respectively. The elongated parallelogram represents the window used for the initial selection of RCGs. Two large circles indicate the RCG selection for the two groups.

properly with $\langle V-I\rangle_{\rm all}$ (in fields BUL_SC5 and BUL_SC37). If there were more than 5 RCGs in a given bin, then we adopted the average colour of these RCGs $\langle V-I\rangle_{\rm RC}$, which were estimated in the third paragraph of this section, as the mean colour of RCGs for this bin. Otherwise these bins are filled by the average value of the neighbours. $\langle V-I\rangle_{\rm RC}$ in each bin can not be used for the case (3), because stars reddened by bright red stars contaminate the RCG region in the CMD.

Problematic bins are flagged with "-1" (1), "-2" (2), "-3" (3) and "-4" (4). If $\langle V-I\rangle_{\rm RC}$ is adopted in a bin then this bin is flagged with the above value plus "-10".

We do not have confidence in measurements of $\langle V-I\rangle_{\rm RC}$ at $\langle V-I\rangle_{\rm RC}>4$, where the detection limit makes RCG centroid in the CMD systematically brighter and bluer. This implies that for $\langle V-I\rangle_{\rm RC}>4$ mag our maps give a lower limit to the extinction. We added "-20" to the value of the flag of such bins. Only BUL_SC5 and BUL_SC37 suffer from this effect.

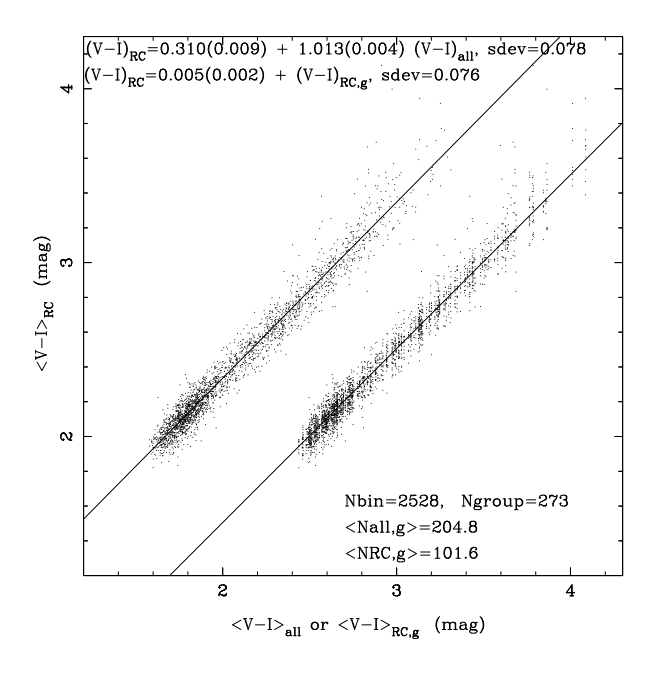


Figure 6. The mean colour of RCGs $(V-I)_{\rm RC}$ in each bin as a function of the mean colour of all stars in the bin $((V-I)_{\rm all},$ upper sequence) and the mean colour of RCGs in each group $((V-I)_{\rm RC,g},$ lower sequence) in the field BUL_SC22. $(V-I)_{\rm RC,g}$ is shifted by +0.5 mag for clarity.

4.2 Zero point

We assume that the average colour of RCG stars, corrected for interstellar reddening, is the same in every field, and we ignore a possible weak dependence on metalicity (Paczyński & Stanek 1998). The zero-point of $\langle V-I\rangle_{0,\rm RC}$ is calibrated following Alcock et al. (1998b). In Fig. 7, we show the offset of our relative extinction $A_{V,\rm RC}$ and V-band absolute extinction for 20 RRab in Alcock et al. (1998b), $A_{V,\rm RR}$. The average offset is $\langle A_{V,\rm RC} - A_{V,\rm RR} \rangle = 0.055 \pm 0.048$ with the standard deviation of sdev=0.22. The errors and sdev are the same as in Alcock et al. (1998b) with Stanek (1996)'s map. This means that reddening corrected $\langle V-I \rangle$ colour and $\langle I \rangle$ magnitude of RCGs are given as $1+0.055/R_{VI}=1.028$ and the value of $I_{0,\rm RC}$ in table 2 plus $0.055R_I/R_{VI}=0.027$, respectively. The extinction corrected I-band magnitudes $I_{0,\rm RC}^*$ after zero-point correction are shown in table 2.

Our extinction and reddening maps are calibrated by this offset. We show the A_V extinction maps in Fig. 8. The parameters: the bin-size, the number of groups, the total number of all stars, the average number of all stars in each bin, the total number of RCGs, the average number of RCGs in each group, the average values and errors in E(V-I), A_V and A_I are given in Table 3. The values of $\langle \sigma \rangle$ are the statistical errors in relative maps, and they do not include zero-point errors $\sigma_{E(V-I),0}=0.024$, $\sigma_{A_V,0}=0.048$ and $\sigma_{A_I,0}=0.024$. To check our maps we present in Fig. 9 a comparison of A_V in the relatively large overlap region of BUL_SC30 and BUL_SC31. One can see a good correlation between them in this figure, and $\chi^2/d.o.f.=1.15$ implies that our error estimate is reasonable.

Table 3. Basic parameters of maps, the bin-size, the number of groups, the total number of all stars, the mean number of all stars in each bin, the total number of RCGs, mean of RCGs in each group, the mean of values and errors in E(V-I), A_V and A_I .

| Total Mean Lotal Mean Lotal Mean Mean Lotal Mean Mean Lotal L | BUL | binsize | $N_{ m grp}$ | N_{a} | 11 | N | RC | E(V | (-I) | A_V | | Δ | A_I | |
|---|-----|---------|--------------|------------------|-------|-------|------|-------|-------|-------|-------|-------|-------|--|
| 1 73.1 189 647014 203.1 18571 98.3 0.854 0.012 1.677 0.027 0.823 0.017 2 68.3 207 753366 198.4 20416 98.6 0.787 0.012 1.545 0.024 0.759 0.013 3 73.1 427 653389 205.3 42183 98.8 1.472 0.014 2.891 0.065 1.419 0.061 4 70.6 417 693066 197.7 41059 98.5 1.319 0.014 2.591 0.054 1.272 0.048 5 157.5 - 145562 209.2 21310 35.6 2.918 0.030 5.733 0.192 2.814 0.184 6 107.8 68 319093 221.0 6783 99.8 0.700 0.011 1.327 0.025 0.652 0.015 7 97.5 62 376688 210.3 6176 99.6 0.676 0.012 1.327 0.025 0.652 0.015 8 113.8 52 287663 214.7 4476 86.1 1.087 0.014 2.135 0.042 1.048 0.034 9 113.8 50 269318 197.2 4516 99.3 1.060 0.013 2.083 0.093 1.023 0.032 10 107.8 61 316050 219.4 5382 88.2 1.136 0.013 2.083 0.093 1.033 0.032 11 113.8 58 287074 220.4 4965 85.6 1.153 0.014 2.266 0.046 1.112 0.039 12 93.1 84 400853 215.7 7154 85.2 1.165 0.015 2.289 0.048 1.123 0.040 13 89.0 83 455162 212.6 7088 85.4 1.047 0.015 2.286 0.042 1.009 0.034 14 93.1 158 409086 201.4 15727 99.5 1.269 0.012 2.494 0.048 1.23 0.040 15 102.4 134 322254 221.3 13232 98.8 1.408 0.012 2.766 0.059 1.358 0.055 16 89.0 127 444114 232.1 11926 93.9 1.094 0.013 2.150 0.038 1.055 0.031 17 85.3 131 494911 213.3 12606 96.2 0.988 0.012 1.940 0.031 0.952 0.022 18 73.1 189 649856 196.7 18267 96.7 0.904 0.012 1.767 0.028 0.872 0.019 19 75.9 173 625566 203.6 16562 95.7 1.022 0.012 2.008 0.034 0.986 0.026 20 68.3 313 732180 193.8 30732 98.2 0.986 0.013 1.936 0.032 0.951 0.023 21 66.1 287 793369 197.6 27964 97.4 0.930 0.013 1.827 0.030 0.897 0.020 22 75.9 273 596019 194.3 26357 96.5 1.392 0.013 2.734 0.060 1.342 0.055 23 78.8 230 583168 204.6 22400 97.4 1.377 0.013 2.704 0.068 1.327 0.053 24 81.9 228 509439 196.1 22737 99.7 1.282 0.011 2.519 0.049 1.237 0.045 25 81.9 210 519559 198.7 20908 9.6 1.191 0.011 2.339 0.042 1.148 0.037 27 75.9 156 594953 193.9 15333 98.3 0.860 0.011 1.690 0.025 0.830 0.016 28 102.4 80 339107 201.0 7871 98.4 0.834 0.012 1.609 0.025 0.830 0.016 28 102.4 80 339107 201.0 7871 98.4 0.834 0.012 1.614 0.025 0.792 0.011 | | | 1 'grp | | | | | , | , | | | | | |
| 2 68.3 207 753366 198.4 20416 98.6 0.787 0.012 1.545 0.024 0.759 0.061 3 73.1 427 653389 205.3 42183 98.8 1.472 0.014 2.891 0.065 1.272 0.048 5 157.5 - 145662 209.2 21310 35.6 2.918 0.030 5.733 0.192 2.814 0.184 6 107.8 68 319093 221.0 6783 99.8 0.700 0.011 1.374 0.024 0.675 0.015 7 97.5 62 376688 210.3 6176 99.6 0.676 0.012 1.327 0.025 0.652 0.015 8 113.8 50 269318 197.2 4456 86.1 1.060 0.013 2.933 0.042 1.048 0.037 11 113.8 50 269318 197.2 291.4 5382 88.2 <td></td> <td>- ,</td> <td>180</td> <td>647014</td> <td>202.1</td> <td>18571</td> <td>08.3</td> <td>0.854</td> <td></td> <td>1 677</td> <td></td> <td>0.853</td> <td></td> | | - , | 180 | 647014 | 202.1 | 18571 | 08.3 | 0.854 | | 1 677 | | 0.853 | | |
| 3 73.1 427 653389 205.3 42183 98.8 1.472 0.014 2.891 0.065 1.419 0.061 4 70.6 417 693066 197.7 41059 98.5 1.319 0.014 2.591 0.064 1.272 0.048 5 157.5 - 145562 209.2 21310 35.6 2.918 0.030 5733 0.192 2.814 0.044 6 107.8 68 319093 221.0 6783 99.8 0.700 0.011 1.374 0.024 0.675 0.015 8 113.8 52 287653 214.7 4476 86.1 1.087 0.014 2.135 0.042 1.048 0.032 10 107.8 61 316050 219.4 5382 88.2 1.136 0.013 2.231 0.044 1.095 0.037 11 113.8 54 28053 215.7 7154 85.4 1.047 <td></td> | | | | | | | | | | | | | | |
| 4 70.6 417 693066 197.7 41059 98.5 1.319 0.014 2.591 0.054 1.272 0.048 5 157.5 - 145562 209.2 21310 35.6 2.918 0.030 5.733 0.192 2.814 0.184 6 107.8 68 31903 221.0 6783 98.8 0.700 0.011 1.374 0.025 0.652 0.015 7 97.5 62 376688 210.3 6176 99.6 0.676 0.012 1.327 0.025 0.652 0.015 8 113.8 50 269318 197.2 4476 86.1 1.087 0.014 2.135 0.042 1.048 0.034 10 107.8 61 316050 219.4 5382 88.2 1.136 0.013 2.033 0.044 1.095 0.037 11 113.8 490853 215.7 7154 85.2 1.166 2.206< | | | | | | | | | | | | | | |
| 5 157.5 - 145562 209.2 21310 35.6 2.918 0.030 5.733 0.192 2.814 0.184 6 107.8 68 319093 221.0 6783 99.8 0.700 0.011 1.374 0.025 0.652 0.015 7 97.5 62 376688 210.3 6116 99.6 0.676 0.012 1.327 0.025 0.652 0.013 8 113.8 50 269318 197.2 4516 90.3 1.060 0.013 2.033 0.039 1.023 0.032 10 107.8 61 31605 219.4 4865 8.6 1.153 0.014 2.266 0.046 1.112 0.039 11 113.8 58 287074 220.4 4965 85.6 1.153 0.014 2.266 0.046 1.112 0.039 13 88.90 83 455162 212.6 70.88 85.4 1.067 <td></td> | | | | | | | | | | | | | | |
| 6 107.8 68 319093 221.0 6783 99.8 0.700 0.011 1.374 0.024 0.675 0.015 7 97.5 62 376688 210.3 6176 99.6 0.676 0.012 1.327 0.025 0.652 0.013 8 113.8 50 269318 197.2 4516 90.3 1.060 0.013 2.083 0.039 1.023 0.032 10 107.8 61 316050 219.4 5382 88.2 1.136 0.013 2.281 0.044 1.095 0.033 11 113.8 58 287074 220.4 4965 85.6 1.153 0.014 1.099 0.041 1.099 0.041 1.099 0.041 1.099 0.042 1.099 0.041 1.009 0.041 1.099 0.042 1.090 0.044 1.049 0.042 1.099 0.042 2.494 0.048 1.224 0.044 1.049 0.043 <td></td> | | | | | | | | | | | | | | |
| 7 97.5 62 376688 210.3 6176 99.6 0.676 0.012 1.327 0.025 0.652 0.015 8 113.8 52 287653 214.7 4476 86.1 1.087 0.014 2.135 0.042 1.048 0.032 10 107.8 61 316050 219.4 5382 88.2 1.136 0.013 2.231 0.044 1.095 0.037 11 113.8 58 287074 220.4 4965 85.6 1.153 0.014 2.266 0.046 1.112 0.039 12 93.1 84 400853 215.7 7154 85.2 1.165 0.015 2.289 0.048 1.123 0.049 13 89.0 83 455162 212.6 7088 85.4 1.047 0.012 2.494 0.048 1.224 0.044 14 93.1 158 490856 201.4 15727 99.5 1.269 </td <td></td> | | | | | | | | | | | | | | |
| 8 113.8 52 287653 214.7 4476 86.1 1.087 0.014 2.135 0.042 1.048 0.034 9 113.8 50 269318 197.2 4516 90.3 1.060 0.013 2.083 0.039 1.023 0.032 11 107.8 61 316050 219.4 4965 85.6 1.153 0.014 2.266 0.044 1.093 12 93.1 84 400853 215.7 7154 85.2 1.165 0.015 2.289 0.048 1.123 0.040 13 89.0 83 455162 212.6 7088 85.4 1.047 0.015 2.289 0.048 1.223 0.044 13 89.0 83 455162 212.6 7088 85.4 1.047 0.012 2.766 0.042 1.009 0.034 14 93.1 158 49086 201.3 13232 98.8 1.408 0.012 <td></td> | | | | | | | | | | | | | | |
| 9 113.8 50 269318 197.2 4516 90.3 1.060 0.013 2.083 0.039 1.023 0.032 10 107.8 61 316050 219.4 5382 88.2 1.136 0.013 2.236 0.044 1.095 0.037 11 113.8 58 287074 220.4 4965 85.6 1.153 0.014 2.266 0.046 1.112 0.039 12 93.1 84 400853 215.7 7154 85.2 1.165 0.015 2.266 0.048 1.123 0.040 13 89.0 83 455162 212.6 7088 85.4 1.047 0.015 2.056 0.042 1.009 0.031 15 409086 201.4 15727 99.5 1.269 0.012 2.444 0.042 1.022 0.012 2.766 0.059 1.358 0.055 16 89.0 127 444114 232.1 | | | | | | | | | | | | | | |
| 10 | | | | | | | | | | | | | | |
| 11 113.8 58 287074 220.4 4965 85.6 1.153 0.014 2.266 0.046 1.112 0.039 12 93.1 84 400853 215.7 7154 85.2 1.165 0.015 2.289 0.048 1.123 0.040 13 89.0 83 455162 212.6 7088 85.4 1.047 0.015 2.289 0.042 1.009 0.034 14 93.1 158 409086 201.4 15727 99.5 1.269 0.012 2.494 0.048 1.224 0.044 15 102.4 134 322254 221.3 13232 98.8 1.408 0.012 2.766 0.059 1.358 0.055 16 89.0 127 444114 232.1 11926 93.9 1.094 0.012 1.766 0.059 1.052 0.031 17 85.3 131 494914 213.3 1.2667 96.7 <td< td=""><td></td><td></td><td></td><td></td><td></td><td></td><td></td><td></td><td></td><td></td><td></td><td></td><td></td></td<> | | | | | | | | | | | | | | |
| 12 93.1 84 400853 215.7 7154 85.2 1.165 0.015 2.289 0.048 1.123 0.040 13 89.0 83 455162 212.6 7088 85.4 1.047 0.015 2.056 0.042 1.009 0.034 14 93.1 158 409086 201.4 15727 99.5 1.269 0.012 2.494 0.048 1.224 0.044 15 102.4 134 322254 221.3 13232 98.8 1.408 0.012 2.766 0.059 1.358 0.055 16 89.0 127 444114 232.1 11926 93.9 1.094 0.013 2.150 0.038 1.055 0.031 17 85.3 131 494911 213.3 12606 96.2 0.988 0.012 1.940 0.031 0.952 0.028 18 73.1 189 649856 196.7 18267 96.7 <td< td=""><td></td><td></td><td></td><td></td><td></td><td></td><td></td><td></td><td></td><td></td><td></td><td></td><td></td></td<> | | | | | | | | | | | | | | |
| 13 89.0 83 455162 212.6 7088 85.4 1.047 0.015 2.056 0.042 1.009 0.034 14 93.1 158 409086 201.4 15727 99.5 1.269 0.012 2.494 0.048 1.224 0.044 15 102.4 134 322254 221.3 13232 98.8 1.408 0.012 2.766 0.059 1.358 0.055 16 89.0 127 444114 232.1 11926 93.9 1.094 0.013 2.150 0.038 1.055 0.031 17 85.3 131 494911 213.3 12606 96.2 0.988 0.012 1.760 0.028 0.872 0.019 18 73.1 189 649856 196.7 18267 96.7 0.904 0.012 1.776 0.028 0.872 0.019 19 75.9 173 62566 203.6 16562 95.7 <t< td=""><td></td><td></td><td></td><td></td><td></td><td></td><td></td><td></td><td></td><td></td><td></td><td></td><td></td></t<> | | | | | | | | | | | | | | |
| 14 93.1 158 409086 201.4 15727 99.5 1.269 0.012 2.494 0.048 1.224 0.044 15 102.4 134 322254 221.3 13232 98.8 1.408 0.012 2.766 0.059 1.358 0.055 16 89.0 127 444114 232.1 11926 93.9 1.094 0.013 2.150 0.038 1.055 0.031 17 85.3 131 494911 213.3 12606 96.2 0.988 0.012 1.776 0.028 0.872 0.019 19 75.9 173 625566 203.6 16562 95.7 1.022 0.012 2.008 0.034 0.986 0.023 20 68.3 313 732180 193.8 30732 98.2 0.986 0.013 1.827 0.030 0.897 0.022 27 75.9 273 596019 194.3 26357 96.5 | | | | | | | | | | | | | | |
| 15 102.4 134 322254 221.3 13232 98.8 1.408 0.012 2.766 0.059 1.358 0.055 16 89.0 127 444114 232.1 11926 93.9 1.094 0.013 2.150 0.038 1.055 0.031 17 85.3 131 494911 213.3 12606 96.2 0.988 0.012 1.940 0.031 0.952 0.022 18 73.1 189 649856 196.7 18267 96.7 0.904 0.012 1.776 0.028 0.872 0.019 19 75.9 173 625566 203.6 16562 95.7 1.022 0.012 2.008 0.034 0.986 0.026 20 68.3 313 732180 193.8 30732 98.2 0.986 0.013 1.936 0.032 0.951 0.023 21 66.1 287 79369 197.6 27964 97.4 | | | | | | | | | | | | | | |
| 16 89.0 127 444114 232.1 11926 93.9 1.094 0.013 2.150 0.038 1.055 0.031 17 85.3 131 494911 213.3 12606 96.2 0.988 0.012 1.940 0.031 0.952 0.022 18 73.1 189 649856 196.7 18267 96.7 0.094 0.012 1.776 0.028 0.872 0.019 19 75.9 173 625566 203.6 16562 95.7 1.022 0.012 2.008 0.034 0.986 0.023 20 68.3 313 732180 193.8 30732 98.2 0.986 0.013 1.936 0.032 0.951 0.023 21 66.1 287 793369 197.6 27964 97.4 0.930 0.013 1.827 0.030 0.897 0.020 22 75.9 273 596019 194.3 26357 96.5 | | | | | | | | | | | | | | |
| 17 85.3 131 494911 213.3 12606 96.2 0.988 0.012 1.940 0.031 0.952 0.022 18 73.1 189 649856 196.7 18267 96.7 0.904 0.012 1.776 0.028 0.872 0.019 19 75.9 173 625566 203.6 16562 95.7 1.022 0.012 2.008 0.034 0.986 0.026 20 68.3 313 732180 193.8 30732 98.2 0.986 0.013 1.936 0.032 0.951 0.023 21 66.1 287 793369 197.6 27964 97.4 0.930 0.013 1.827 0.030 0.897 0.020 22 75.9 273 596019 194.3 26357 96.5 1.392 0.013 1.827 0.030 0.897 0.020 22 75.9 150 59439 196.1 22737 99.7 < | | | | | | | | | | | | | | |
| 18 73.1 189 649856 196.7 18267 96.7 0.904 0.012 1.776 0.028 0.872 0.019 19 75.9 173 625566 203.6 16562 95.7 1.022 0.012 2.008 0.034 0.986 0.026 20 68.3 313 732180 193.8 30732 98.2 0.986 0.013 1.936 0.032 0.951 0.023 21 66.1 287 793369 197.6 27964 97.4 0.930 0.013 1.827 0.030 0.897 0.020 22 75.9 273 596019 194.3 26357 96.5 1.392 0.013 2.734 0.060 1.342 0.055 23 78.8 230 583168 204.6 22400 97.4 1.377 0.013 2.704 0.058 1.327 0.053 24 81.9 210 519559 198.7 20908 99.6 | | | | | | | | | | | | | | |
| 19 75.9 173 625566 203.6 16562 95.7 1.022 0.012 2.008 0.034 0.986 0.023 20 68.3 313 732180 193.8 30732 98.2 0.986 0.013 1.936 0.032 0.951 0.023 21 66.1 287 793369 197.6 27964 97.4 0.930 0.013 1.827 0.030 0.897 0.020 22 75.9 273 596019 194.3 26357 96.5 1.392 0.013 2.704 0.058 1.342 0.055 23 78.8 230 583168 204.6 22400 97.4 1.377 0.013 2.704 0.058 1.327 0.053 24 81.9 2210 519559 198.7 20908 99.6 1.191 0.011 2.519 0.042 1.148 0.037 26 75.9 156 594953 193.9 15333 98.3 | | | | | | | | | | | | | | |
| 20 68.3 313 732180 193.8 30732 98.2 0.986 0.013 1.936 0.032 0.951 0.023 21 66.1 287 793369 197.6 27964 97.4 0.930 0.013 1.827 0.030 0.897 0.020 22 75.9 273 596019 194.3 26357 96.5 1.392 0.013 2.734 0.060 1.342 0.055 23 78.8 230 583168 204.6 22400 97.4 1.377 0.013 2.704 0.058 1.327 0.053 24 81.9 228 509439 196.1 22737 99.7 1.282 0.011 2.519 0.049 1.237 0.045 25 81.9 210 519559 198.7 20908 99.6 1.191 0.011 1.857 0.029 0.912 0.021 26 75.9 156 594953 193.9 15333 98.3 | | | | | | | | | | | | | | |
| 21 66.1 287 793369 197.6 27964 97.4 0.930 0.013 1.827 0.030 0.897 0.020 22 75.9 273 596019 194.3 26357 96.5 1.392 0.013 2.734 0.060 1.342 0.055 23 78.8 230 583168 204.6 22400 97.4 1.377 0.013 2.704 0.058 1.327 0.053 24 81.9 228 509439 196.1 22737 99.7 1.282 0.011 2.519 0.049 1.237 0.045 25 81.9 210 519559 198.7 20908 99.6 1.191 0.011 2.519 0.042 1.148 0.037 26 75.9 175 617829 201.2 16864 96.4 0.945 0.011 1.857 0.029 0.912 0.021 27 75.9 156 594953 193.9 15333 98.3 0.860 0.011 1.690 0.025 0.830 0.016 28 | | | | | | | | | | | | | | |
| 22 75.9 273 596019 194.3 26357 96.5 1.392 0.013 2.734 0.060 1.342 0.055 23 78.8 230 583168 204.6 22400 97.4 1.377 0.013 2.704 0.058 1.327 0.053 24 81.9 228 509439 196.1 22737 99.7 1.282 0.011 2.519 0.049 1.237 0.045 25 81.9 210 519559 198.7 20908 99.6 1.191 0.011 2.339 0.042 1.148 0.037 26 75.9 156 594953 193.9 15333 98.3 0.860 0.011 1.690 0.025 0.830 0.016 28 102.4 80 339107 201.0 7871 98.4 0.834 0.012 1.638 0.025 0.804 0.015 29 93.1 76 398252 194.7 7430 97.8 <td< td=""><td></td><td></td><td></td><td></td><td></td><td></td><td></td><td></td><td></td><td></td><td></td><td></td><td></td></td<> | | | | | | | | | | | | | | |
| 23 78.8 230 583168 204.6 22400 97.4 1.377 0.013 2.704 0.058 1.327 0.053 24 81.9 228 509439 196.1 22737 99.7 1.282 0.011 2.519 0.049 1.237 0.045 25 81.9 210 519559 198.7 20908 99.6 1.191 0.011 2.339 0.042 1.148 0.037 26 75.9 175 617829 201.2 16864 96.4 0.945 0.011 1.857 0.029 0.912 0.021 27 75.9 156 594953 193.9 15333 98.3 0.860 0.011 1.690 0.025 0.830 0.016 28 102.4 80 339107 201.0 7871 98.4 0.834 0.012 1.638 0.025 0.804 0.015 29 93.1 76 398252 194.7 7430 97.8 0.779 0.011 1.530 0.024 0.751 0.015 30 <t< td=""><td></td><td></td><td></td><td>793369</td><td>197.6</td><td>27964</td><td>97.4</td><td>0.930</td><td>0.013</td><td>1.827</td><td>0.030</td><td></td><td>0.020</td></t<> | | | | 793369 | 197.6 | 27964 | 97.4 | 0.930 | 0.013 | 1.827 | 0.030 | | 0.020 | |
| 24 81.9 228 509439 196.1 22737 99.7 1.282 0.011 2.519 0.049 1.237 0.045 25 81.9 210 519559 198.7 20908 99.6 1.191 0.011 2.339 0.042 1.148 0.037 26 75.9 175 617829 201.2 16864 96.4 0.945 0.011 1.857 0.029 0.912 0.021 27 75.9 156 594953 193.9 15333 98.3 0.860 0.011 1.690 0.025 0.830 0.016 28 102.4 80 339107 201.0 7871 98.4 0.834 0.012 1.638 0.025 0.804 0.015 29 93.1 76 398252 194.7 7430 97.8 0.779 0.011 1.530 0.024 0.751 0.015 30 73.1 258 671739 211.3 25476 98.7 0.971 0.012 1.810 0.028 0.888 0.018 32 <t< td=""><td></td><td>75.9</td><td></td><td>596019</td><td>194.3</td><td>26357</td><td>96.5</td><td></td><td>0.013</td><td>2.734</td><td>0.060</td><td></td><td>0.055</td></t<> | | 75.9 | | 596019 | 194.3 | 26357 | 96.5 | | 0.013 | 2.734 | 0.060 | | 0.055 | |
| 25 81.9 210 519559 198.7 20908 99.6 1.191 0.011 2.339 0.042 1.148 0.037 26 75.9 175 617829 201.2 16864 96.4 0.945 0.011 1.857 0.029 0.912 0.021 27 75.9 156 594953 193.9 15333 98.3 0.860 0.011 1.690 0.025 0.830 0.016 28 102.4 80 339107 201.0 7871 98.4 0.834 0.012 1.638 0.025 0.804 0.015 29 93.1 76 398252 194.7 7430 97.8 0.779 0.011 1.530 0.024 0.751 0.015 30 73.1 258 671739 211.3 25476 98.7 0.971 0.012 1.908 0.030 0.937 0.022 31 70.6 245 716500 204.2 24183 98.7 0.921 0.012 1.810 0.028 0.888 0.018 32 <t< td=""><td></td><td>78.8</td><td></td><td>583168</td><td>204.6</td><td>22400</td><td>97.4</td><td></td><td>0.013</td><td>2.704</td><td>0.058</td><td>1.327</td><td>0.053</td></t<> | | 78.8 | | 583168 | 204.6 | 22400 | 97.4 | | 0.013 | 2.704 | 0.058 | 1.327 | 0.053 | |
| 26 75.9 175 617829 201.2 16864 96.4 0.945 0.011 1.857 0.029 0.912 0.021 27 75.9 156 594953 193.9 15333 98.3 0.860 0.011 1.690 0.025 0.830 0.016 28 102.4 80 339107 201.0 7871 98.4 0.834 0.012 1.638 0.025 0.804 0.015 29 93.1 76 398252 194.7 7430 97.8 0.779 0.011 1.530 0.024 0.751 0.015 30 73.1 258 671739 211.3 25476 98.7 0.971 0.012 1.908 0.030 0.937 0.022 31 70.6 245 716500 204.2 24183 98.7 0.921 0.012 1.810 0.028 0.888 0.018 32 70.6 217 684274 200.0 21387 98.6 <td< td=""><td></td><td>81.9</td><td></td><td>509439</td><td>196.1</td><td>22737</td><td>99.7</td><td></td><td></td><td>2.519</td><td>0.049</td><td>1.237</td><td></td></td<> | | 81.9 | | 509439 | 196.1 | 22737 | 99.7 | | | 2.519 | 0.049 | 1.237 | | |
| 27 75.9 156 594953 193.9 15333 98.3 0.860 0.011 1.690 0.025 0.830 0.016 28 102.4 80 339107 201.0 7871 98.4 0.834 0.012 1.638 0.025 0.804 0.015 29 93.1 76 398252 194.7 7430 97.8 0.779 0.011 1.530 0.024 0.751 0.015 30 73.1 258 671739 211.3 25476 98.7 0.971 0.012 1.908 0.030 0.937 0.022 31 70.6 245 716500 204.2 24183 98.7 0.921 0.012 1.810 0.028 0.888 0.018 32 70.6 217 684274 200.0 21387 98.6 0.822 0.012 1.614 0.025 0.792 0.014 33 73.1 184 669836 202.6 17962 97.6 <td< td=""><td>25</td><td>81.9</td><td>210</td><td>519559</td><td>198.7</td><td>20908</td><td>99.6</td><td>1.191</td><td>0.011</td><td>2.339</td><td>0.042</td><td>1.148</td><td>0.037</td></td<> | 25 | 81.9 | 210 | 519559 | 198.7 | 20908 | 99.6 | 1.191 | 0.011 | 2.339 | 0.042 | 1.148 | 0.037 | |
| 28 102.4 80 339107 201.0 7871 98.4 0.834 0.012 1.638 0.025 0.804 0.015 29 93.1 76 398252 194.7 7430 97.8 0.779 0.011 1.530 0.024 0.751 0.015 30 73.1 258 671739 211.3 25476 98.7 0.971 0.012 1.908 0.030 0.937 0.022 31 70.6 245 716500 204.2 24183 98.7 0.921 0.012 1.810 0.028 0.888 0.018 32 70.6 217 684274 200.0 21387 98.6 0.822 0.012 1.614 0.025 0.792 0.014 33 73.1 184 669836 202.6 17962 97.6 0.865 0.012 1.699 0.026 0.834 0.016 34 64.0 331 849632 198.4 31842 96.2 1.146 0.013 2.252 0.042 1.106 0.035 35 <t< td=""><td>26</td><td>75.9</td><td>175</td><td>617829</td><td>201.2</td><td>16864</td><td>96.4</td><td>0.945</td><td>0.011</td><td>1.857</td><td>0.029</td><td>0.912</td><td>0.021</td></t<> | 26 | 75.9 | 175 | 617829 | 201.2 | 16864 | 96.4 | 0.945 | 0.011 | 1.857 | 0.029 | 0.912 | 0.021 | |
| $\begin{array}{cccccccccccccccccccccccccccccccccccc$ | 27 | 75.9 | 156 | 594953 | 193.9 | 15333 | 98.3 | 0.860 | 0.011 | 1.690 | 0.025 | 0.830 | 0.016 | |
| $\begin{array}{cccccccccccccccccccccccccccccccccccc$ | 28 | 102.4 | 80 | 339107 | 201.0 | 7871 | 98.4 | 0.834 | 0.012 | 1.638 | 0.025 | 0.804 | 0.015 | |
| $\begin{array}{cccccccccccccccccccccccccccccccccccc$ | 29 | 93.1 | 76 | 398252 | 194.7 | 7430 | 97.8 | 0.779 | 0.011 | 1.530 | 0.024 | 0.751 | 0.015 | |
| 32 70.6 217 684274 200.0 21387 98.6 0.822 0.012 1.614 0.025 0.792 0.014 33 73.1 184 669836 202.6 17962 97.6 0.865 0.012 1.699 0.026 0.834 0.016 34 64.0 331 849632 198.4 31842 96.2 1.146 0.013 2.252 0.042 1.106 0.035 35 70.6 221 696335 196.7 21495 97.3 0.936 0.012 1.838 0.029 0.902 0.019 36 68.3 205 764524 201.5 19973 97.4 0.825 0.012 1.621 0.026 0.796 0.015 37 102.4 - 463048 274.3 37114 23.4 1.921 0.029 3.773 0.114 1.852 0.102 38 73.1 213 634009 199.2 21036 98.8 0.927 0.012 1.821 0.029 0.894 0.019 39 | 30 | 73.1 | 258 | 671739 | 211.3 | 25476 | 98.7 | 0.971 | 0.012 | 1.908 | 0.030 | 0.937 | 0.022 | |
| 33 73.1 184 669836 202.6 17962 97.6 0.865 0.012 1.699 0.026 0.834 0.016 34 64.0 331 849632 198.4 31842 96.2 1.146 0.013 2.252 0.042 1.106 0.035 35 70.6 221 696335 196.7 21495 97.3 0.936 0.012 1.838 0.029 0.902 0.019 36 68.3 205 764524 201.5 19973 97.4 0.825 0.012 1.621 0.026 0.796 0.015 37 102.4 - 463048 274.3 37114 23.4 1.921 0.029 3.773 0.114 1.852 0.102 38 73.1 213 634009 199.2 21036 98.8 0.927 0.012 1.821 0.029 0.894 0.019 39 70.6 383 684042 193.9 37753 98.6 1.337 0.013 2.625 0.055 1.289 0.050 40 93.1 230 419439 206.9 22680 98.6 1.496 0.012 2.940 0.066 1.443 0.063 <td>31</td> <td>70.6</td> <td>245</td> <td></td> <td>204.2</td> <td>24183</td> <td>98.7</td> <td>0.921</td> <td>0.012</td> <td>1.810</td> <td>0.028</td> <td>0.888</td> <td>0.018</td> | 31 | 70.6 | 245 | | 204.2 | 24183 | 98.7 | 0.921 | 0.012 | 1.810 | 0.028 | 0.888 | 0.018 | |
| 34 64.0 331 849632 198.4 31842 96.2 1.146 0.013 2.252 0.042 1.106 0.035 35 70.6 221 696335 196.7 21495 97.3 0.936 0.012 1.838 0.029 0.902 0.019 36 68.3 205 764524 201.5 19973 97.4 0.825 0.012 1.621 0.026 0.796 0.015 37 102.4 - 463048 274.3 37114 23.4 1.921 0.029 3.773 0.114 1.852 0.102 38 73.1 213 634009 199.2 21036 98.8 0.927 0.012 1.821 0.029 0.894 0.019 39 70.6 383 684042 193.9 37753 98.6 1.337 0.013 2.625 0.055 1.289 0.050 40 93.1 230 419439 206.9 22680 98.6 1.496 0.012 2.940 0.066 1.443 0.063 | 32 | 70.6 | 217 | 684274 | 200.0 | 21387 | 98.6 | 0.822 | 0.012 | 1.614 | 0.025 | 0.792 | 0.014 | |
| 35 70.6 221 696335 196.7 21495 97.3 0.936 0.012 1.838 0.029 0.902 0.019 36 68.3 205 764524 201.5 19973 97.4 0.825 0.012 1.621 0.026 0.796 0.015 37 102.4 - 463048 274.3 37114 23.4 1.921 0.029 3.773 0.114 1.852 0.102 38 73.1 213 634009 199.2 21036 98.8 0.927 0.012 1.821 0.029 0.894 0.019 39 70.6 383 684042 193.9 37753 98.6 1.337 0.013 2.625 0.055 1.289 0.050 40 93.1 230 419439 206.9 22680 98.6 1.496 0.012 2.940 0.066 1.443 0.063 | 33 | 73.1 | 184 | 669836 | 202.6 | 17962 | 97.6 | 0.865 | 0.012 | 1.699 | 0.026 | 0.834 | 0.016 | |
| 36 68.3 205 764524 201.5 19973 97.4 0.825 0.012 1.621 0.026 0.796 0.015 37 102.4 - 463048 274.3 37114 23.4 1.921 0.029 3.773 0.114 1.852 0.102 38 73.1 213 634009 199.2 21036 98.8 0.927 0.012 1.821 0.029 0.894 0.019 39 70.6 383 684042 193.9 37753 98.6 1.337 0.013 2.625 0.055 1.289 0.050 40 93.1 230 419439 206.9 22680 98.6 1.496 0.012 2.940 0.066 1.443 0.063 | 34 | 64.0 | 331 | 849632 | 198.4 | 31842 | 96.2 | 1.146 | 0.013 | 2.252 | 0.042 | 1.106 | 0.035 | |
| 37 102.4 - 463048 274.3 37114 23.4 1.921 0.029 3.773 0.114 1.852 0.102 38 73.1 213 634009 199.2 21036 98.8 0.927 0.012 1.821 0.029 0.894 0.019 39 70.6 383 684042 193.9 37753 98.6 1.337 0.013 2.625 0.055 1.289 0.050 40 93.1 230 419439 206.9 22680 98.6 1.496 0.012 2.940 0.066 1.443 0.063 | 35 | 70.6 | 221 | 696335 | 196.7 | 21495 | 97.3 | 0.936 | 0.012 | 1.838 | 0.029 | 0.902 | 0.019 | |
| 38 73.1 213 634009 199.2 21036 98.8 0.927 0.012 1.821 0.029 0.894 0.019 39 70.6 383 684042 193.9 37753 98.6 1.337 0.013 2.625 0.055 1.289 0.050 40 93.1 230 419439 206.9 22680 98.6 1.496 0.012 2.940 0.066 1.443 0.063 | 36 | 68.3 | 205 | 764524 | 201.5 | 19973 | 97.4 | 0.825 | 0.012 | 1.621 | 0.026 | 0.796 | 0.015 | |
| 39 70.6 383 684042 193.9 37753 98.6 1.337 0.013 2.625 0.055 1.289 0.050 40 93.1 230 419439 206.9 22680 98.6 1.496 0.012 2.940 0.066 1.443 0.063 | 37 | 102.4 | - | 463048 | 274.3 | 37114 | 23.4 | 1.921 | 0.029 | 3.773 | 0.114 | 1.852 | 0.102 | |
| 39 70.6 383 684042 193.9 37753 98.6 1.337 0.013 2.625 0.055 1.289 0.050 40 93.1 230 419439 206.9 22680 98.6 1.496 0.012 2.940 0.066 1.443 0.063 | 38 | 73.1 | 213 | 634009 | 199.2 | 21036 | 98.8 | 0.927 | 0.012 | 1.821 | 0.029 | 0.894 | 0.019 | |
| | | | 383 | 684042 | 193.9 | 37753 | 98.6 | 1.337 | 0.013 | 2.625 | 0.055 | 1.289 | 0.050 | |
| | 40 | 93.1 | 230 | 419439 | 206.9 | 22680 | 98.6 | 1.496 | 0.012 | 2.940 | 0.066 | 1.443 | 0.063 | |
| 41 85.3 229 495001 205.2 22661 99.0 1.351 0.012 2.653 0.055 1.303 0.051 | 41 | 85.3 | 229 | 495001 | 205.2 | 22661 | 99.0 | 1.351 | 0.012 | 2.653 | 0.055 | 1.303 | 0.051 | |
| $42 \qquad 81.9 \qquad 160 521529 198.2 14804 92.5 1.164 0.013 2.286 0.043 1.122 0.036$ | 42 | 81.9 | 160 | 521529 | 198.2 | 14804 | 92.5 | 1.164 | 0.013 | 2.286 | 0.043 | 1.122 | 0.036 | |
| 43 120.5 247 257326 216.0 25921 104.9 1.870 0.012 3.674 0.097 1.803 0.094 | | | | | | | | | | | | | | |
| 44 53346 - 1257 | | | | | | | | | | | | | | |
| 45 78.8 175 562718 205.4 17247 98.5 0.836 0.012 1.642 0.028 0.806 0.018 | | | | | | | | | | | | | 0.018 | |
| 46 85.3 159 495299 213.1 15643 98.4 0.871 0.012 1.711 0.029 0.840 0.019 | | | | | | | | | | | | | | |
| 47 128.0 58 209811 194.4 4986 86.0 1.321 0.015 2.595 0.056 1.274 0.049 | | | | | | | | | | | | | | |
| 48 128.0 57 217083 201.0 5229 91.7 1.194 0.014 2.346 0.046 1.152 0.039 | | | | | | | | | | | | | | |
| 49 136.5 43 193318 203.5 4086 95.0 1.063 0.014 2.089 0.038 1.025 0.030 | | | | | | | | | | | | | | |
| Note: $\langle \sigma \rangle$ do not include zero-point errors $\sigma_{E(V-I),0} = 0.024$, $\sigma_{A_V,0} = 0.048$ and $\sigma_{A_I,0} = 0.024$. | - | | | | | | | | | | | | | |

We show the histogram of E(V-I) for all our maps in Fig. 10. The vertical line indicates the threshold value $E(V-I)_{\rm th}=3.0$, which corresponds to $\langle V-I\rangle_{\rm RC}=4$ mag. We have confidence in our maps below this threshold. However, small, very heavily obscured regions are above this reddening threshold, pushing some RCGs below the OGLE-II detection limit, and distorting the RCGs. This implies that for $\langle V-I\rangle_{\rm RC}>4$ mag our maps give a lower limit to the extinction. Histograms of A_V and A_I can be obtained

by multiplying E(V-I) by R_{VI} and R_I respectively. The thresholds are: $A_{V,\rm th}=5.8$ and $A_{I,\rm th}=2.9$.

The reddening corrected value of $(V-I)_{0,\rm RC}$ may vary from one field to another due to weak dependence on metalicity. The RR Lyrae variables are good distance indicators (e.g., Nemec, Nemec & Lutz 1994) whose period-luminosity relations are well established (Jones, Carney, Storm & Latham 1992). The RR Lyrae lie in the instability strip, the range of their colour is small and

8

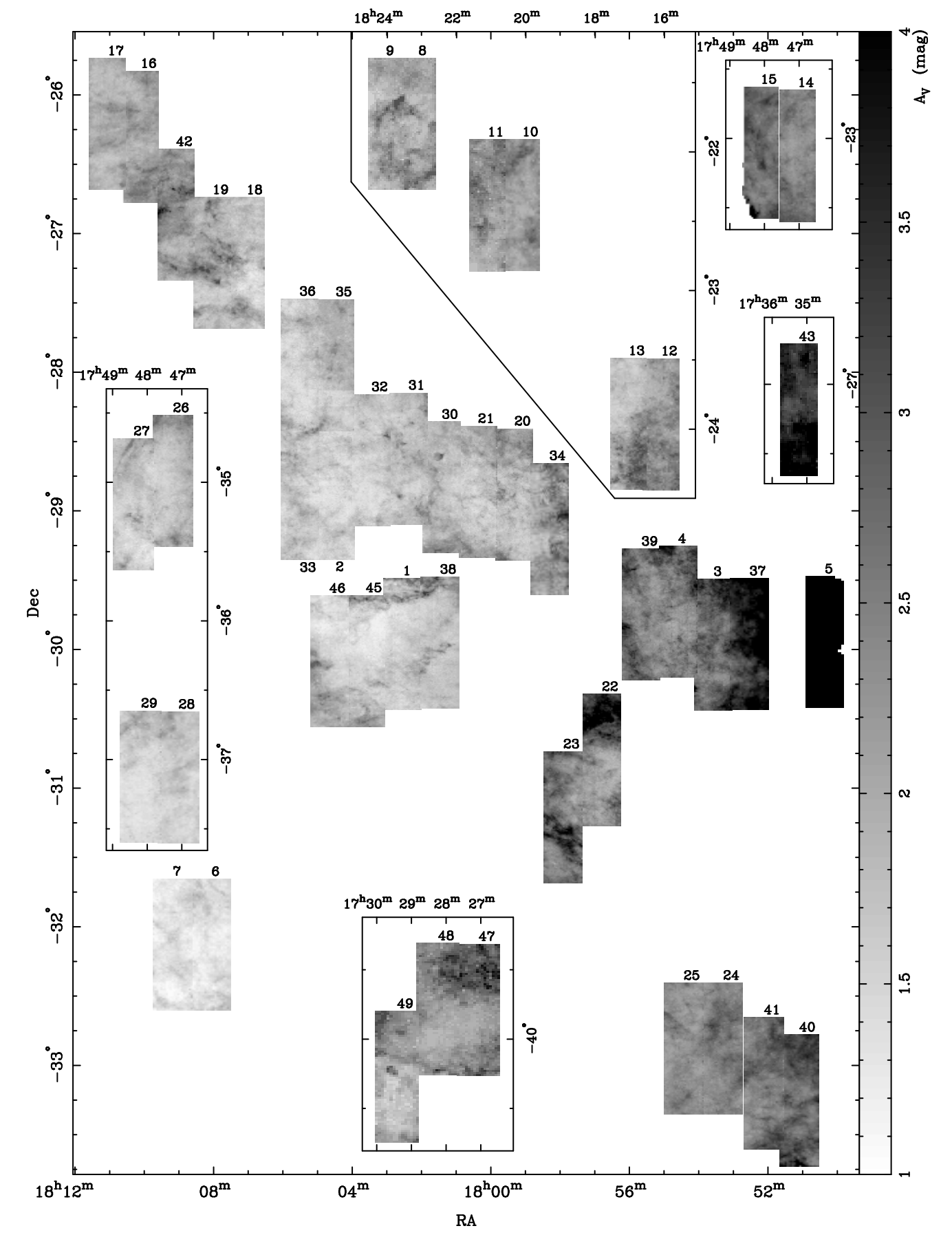


Figure 8. A_V Extinction map. Distant fields are in small boxes. Gray scale is shown at the right corner.

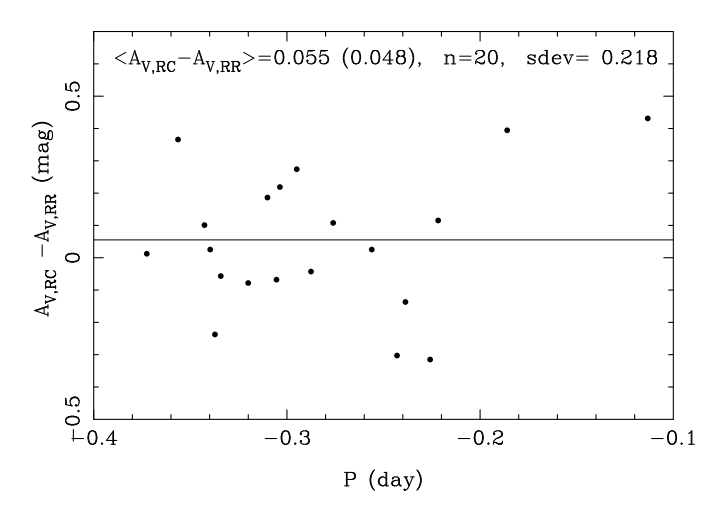


Figure 7. Difference of relative extinction $A_{V,\rm RC}$ from RCGs (see §4.1) and V-band extinction from 20 RRab in Alcock et al. (1998b), $A_{V,\rm RR}$, i.e., the same figure as Fig. 3 of Alcock et al. (1998b).

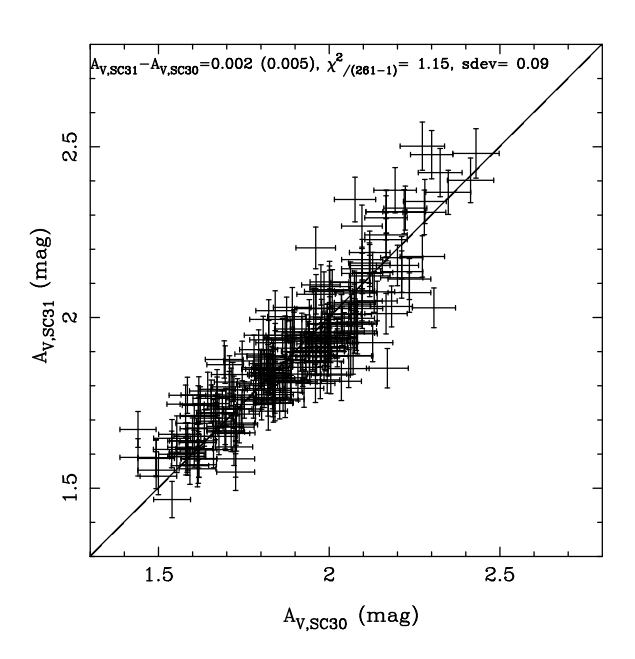


Figure 9. Comparison of A_V of overlap region in BUL_SC30 and in BUL_SC31.

it weakly depends on period, amplitude and/or metallicity (Bono, & Stellingwerf 1994; Alcock et al. 1998a). To check the relative zero-points of our reddening maps for each field we make use of the V-I colour of RR Lyrae Type ab (RRab), assuming that period - $(V-I)_0$ colour relation of RRab is the same for all OLGE-II fields

We selected RRab in OGLE-II Galactic Bulge variable star catalogue (Woźniak et al. 2001) by using the method of Alard (1996). We measured periods P using PDM algorithm (Stellingwerf 1978) and Fourier coefficients by fitting Fourier series with five harmonics. In Fig 11 we show the the amplitude ratio $R_{21} \equiv A_2/A_1$ versus phase differences

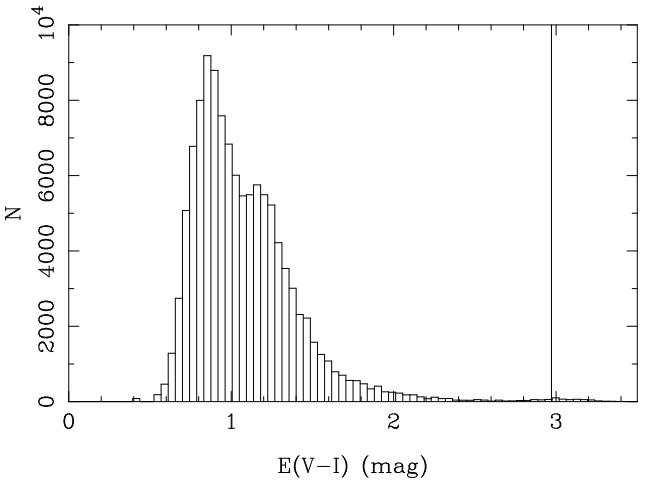


Figure 10. A histogram of E(V-I) for all our maps. Vertical line indicates the threshold value $E(V-I)_{\rm th}=3.0$ mag.

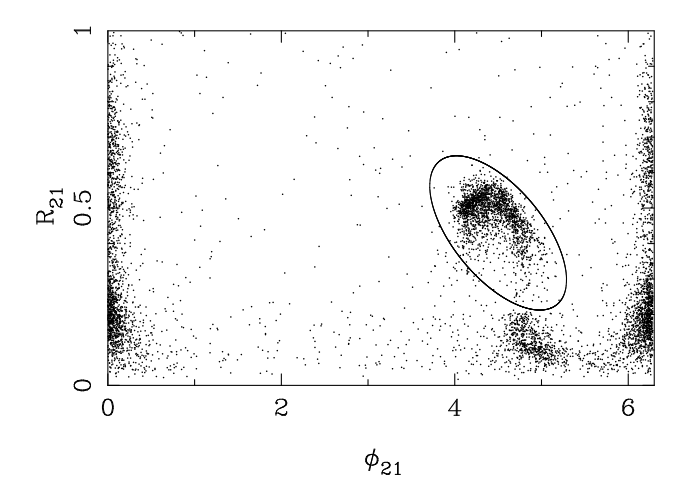


Figure 11. R_{21} v.s. ϕ_{21} for periodic variables in the OGLE catalogue. RRab variables are selected within the ellipse. There is a clump of RRc variables below the ellipse, but we do not use them in this work.

 $\phi_{21}\equiv\phi_2-2\phi_1$ for variables with P<0.9 days, except 0.4985< P<0.5001 days, which are affected by aliasing. We selected 1,961 RRab stars as a clear clump within the ellipse in this figure. Of these 1,819 stars have $\langle V\rangle$ and $\langle I\rangle$ photometry provided by Udalski (2003). We visually inspected all light curves and several stars with non RR Lyrae shape light curves were rejected. In Fig 12 we present colour - magnitude diagram for RRab stars so selected. The differential reddening is apparent. A similar reddening slope is found in §3.

In the following analysis we rejected 39 stars with I < 1.1(V-I)+13.1 because they are either nearby disk stars or they are blended with other bright stars. We did not reject several background RRab below the sequence as they made no difference to our analysis, for which we used 1,780 RRab stars.

We assume that reddening corrected colour $(V-I)_{0,RR}$

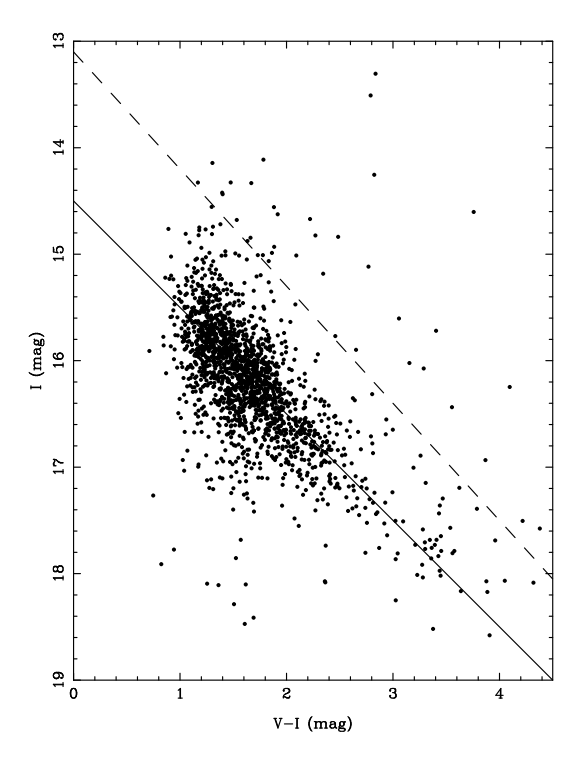


Figure 12. The CMD for RRab variables. Solid line with a slope of I/(V-I)=1.0 is shown as a reference. RRab variables above the dashed line: I=1.1(V-I)+13.1 are rejected in our analysis because they are foreground disk stars or variables blended with other bright stars.

is the same in every field, with a possible weak dependence on period P, or amplitude A, or both. We estimate the zero-points C_i for each field i by fitting extinction corrected colour of RRab with a linear dependence on $\log P$, A, and on both of them. We obtained the following relations:

$$(V - I)_{0,RR} = 0.309(\pm 0.049)\log P + C_i, sdev = 0.158(6)$$

$$(V - I)_{0,RR} = -0.096(\pm 0.016)A + C_i, sdev = 0.157, (7)$$

$$(V - I)_{0,RR} = 0.211(\pm 0.056)\log P - 0.063(\pm 0.018)A$$

$$+ C_i, sdev = 0.156.$$

$$(8)$$

All three relations provided almost the same values of C_i . Fitting with both P and A seems to be an overparameterization.

In Fig. 13, we show extinction corrected colours of RCGs $(V-I)_{0,RC}$ (open circle) and RRab $(V-I)_{0,RR}$ (filled circle and errors) as a function of the galactic l and b, where $(V-I)_{0,RC}$ are measured by the method [3] in § 3 and $(V-I)_{0,RR}$ are the value given by Eq. (6) at $\log P = -0.3$.

 $(V-I)_{0,\mathrm{RC}}$ is constant as assumed. The mean of $(V-I)_{0,\mathrm{RC}}=1.0283\pm0.024$, where we used $\sigma_{E(V-I),0}=0.024$ as the error in $(V-I)_{0,\mathrm{RC}}$, is consistent with the colour of nearby RCGs $(V-I)_{0,\mathrm{RC},\mathrm{near}}=1.01\pm0.08$ mag (Paczyński & Stanek 1998), contrary to $(V-I)_{0,\mathrm{RC},\mathrm{bulge}}=1.11\pm0.12$ by Paczyński et al. (1999) with Stanek (1996)'s map.

 $(V-I)_{0,\mathrm{RR}}$ seems to be systematically redder by about ~ 0.1 mag at large |l|. Such trend can not be seen in b. We plot $(V-I)_{0,\mathrm{RR}}$ as a function |l| in Fig. 14 and we fit it

with a straight line for |l|<6 (filled circle and solid line) and for |l|>6 (open circle and dashed line). One can see the RRab colour is constant at |l|<6 and have a significant (3σ) dependence on |l| at |l|>6. The mean $(V-I)_{0,\rm RR}$ is 0.4670 ± 0.0047 with sdev=0.0286 for |l|<6 and 0.5386 ± 0.0126 with sdev=0.0773 for |l|>6. The significance of the redder colour in |l|>6 is estimated to be 5.3σ level.

This implies that $(V-I)_{0,\mathrm{RC}}$, $(V-I)_{0,\mathrm{RR}}$ or both of them, may vary with l. If we assume that $(V-I)_{0,\mathrm{RR}}$ is constant, then the intrinsic colour of RCGs would be bluer, i.e., the zero-points of our reddening maps would be smaller by ~ 0.1 mag at |l|=10, compared to $|l|\leq 6$. This could be explained if the outer RCGs have lower metalicity and are somewhat bluer than near the Galactic Center. The colour of RRab $(V-I)_{0,\mathrm{RR}}=0.4\sim 0.5$ for $|l|\leq 6$ is consistent with the colour of local RRab, while the two sets of colours were claimed to be different by Stanek (1996)'s map by Stutz, Popowski & Gould 1999.

The scatter of $(V-I)_{0,\rm RR}$ values is large because public domain V-band OGLE photometry is the average of randomly distributed small number of V-band measurements, while the V amplitude is large. Furthermore the scatter is larger for |l|>6 because the number of RRab is small in these fields. Therefore, we do not correct for the offsets apparent in Fig. 13. It will be possible to improve the accuracy of $(V-I)_{0,\rm RR}$ when individual V-band measurements become available.

5 DISCUSSION AND CONCLUSION

We confirmed the anomalous reddening, i.e. a small value of the ratio of total to selective extinction $R_{VI}=1.9\sim2.1$ depending on the line of sight, as measured by Udalski (2003). This implies that the distribution of dust grains may be tipped to smaller sizes in these regions, compared to average in the Galaxy. A detailed analysis of these results is beyond the scope of the present study.

By adopting the mean value of $R_{VI}=1.964$, we have constructed reddening E(V-I) and extinctions, A_V and A_I maps in 48 OGLE-II GB fields, covering a range of $-11^{\circ} < l < 11^{\circ}$, with the total area close to 11 square degrees. The reddening E(V-I) and extinctions, A_V and A_I are measured in the range 0.42 < E(V-I) < 3.5 mag, $0.83 < A_V < 6.9$ mag and $0.41 < A_I < 3.4$. Note: above the threshold values $E(V-I)_{\rm th}=3.0$, $A_{V,\rm th}=5.8$ and $A_{I,\rm th}=2.9$, which correspond to $\langle V-I\rangle_{\rm RC}=4$ mag, our maps give the lower limit to reddening and extinction. Spatial resolutions of maps are $26.7''\sim 106.8''$ depending on the stellar density of each field.

The absolute zero-point is calibrated using 20 RRab variables in Baade's Window, following Alcock et al. (1998b). Relative zero-points of our maps are verified with 1,780 RRab variables found in our fields. We found that these zero-points may be lower by ~ 0.1 mag at larger Galactic longitudes |l| > 6. Note that our extinction map is OK in terms of the relative extinction within each field. The relative zero points are also OK between fields for |l| < 6. We did not make any correction for this effect in the paper.

We used the mean value of $R_{VI} = 1.964$, but different fields have a range of values, with a standard deviation $sdev \sim 0.085$ (see Fig.3). We estimated the errors of our

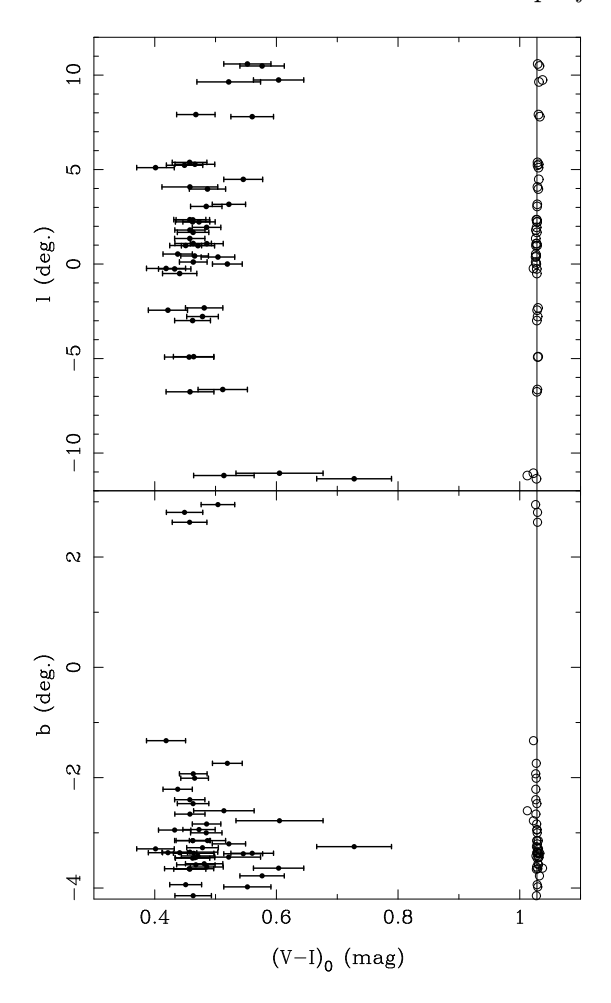


Figure 13. Extinction corrected colours of RCGs $(V-I)_{0,RC}$ (open circle) and RRab $(V-I)_{0,RR}$ (filled circle and errors) as a function of the galactic l and b. $(V-I)_{0,RR}$ are the value given by Eq. (6) at $\log P = -0.3$. Solid line represent a mean of $(V-I)_{0,RC} = 1.0283 \pm 0.024$, sdev = 0.0034, where the error in $(V-I)_{0,RC}$ is dominated by $\sigma_{E(V-I),0} = 0.024$.

maps by taking this range into account. The errors approach 0.17 mag at the highest extinction $(A_V = 6)$.

As noted by Udalski et al. (2002) and Udalski (2003), the I-band filter used by OGLE-II has the red wing somewhat wider than standard. This may lead to systematic deviations from the standard values for very red stars, giving brighter I-band magnitudes (redder V-I colour) for the OGLE-II filter for very red stars (V - I > 2), while the error is negligible in the range where the OGLE-II data were calibrated by standards, i.e. for (V - I < 2). This effect may reach ~ 0.2 mag for the very red RCGs (V - I > 4 mag). This effect makes the slope of reddening line in the CMD somewhat shallower, as shown by Udalski (2003). This effect is not sufficient to explain the anomalous extinction towards the GC. Udalski (2003) analyzed the differences between OGLE-II and standard I-band filters using Kurucz (1992)'s model atmosphere of a typical RCGs, reddened with the standard interstellar extinction of Cardelli, Clayton& Mathis (1989) and Fitzpatrick (1999). He found possible errors to be at the level ± 0.1 in R_{VI} , de-

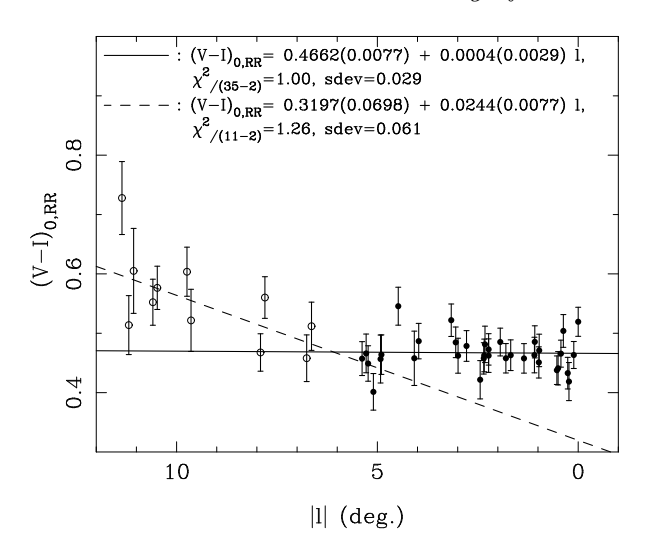


Figure 14. Extinction corrected colours of RRab $(V-I)_{0,RR}$ as a function of the absolute galactic |l|. $(V-I)_{0,RR}$ are the value given by Eq. (6) at $\log P = -0.3$. Filled and open circles represent plots in |l| < 6 and in |l| > 6, and solid and dashed lines indicate the best fits for them, respectively. One can see the RRab colour is constant at |l| < 6 and significantly red at |l| > 6.

pending on the model of extinction and the colour range of RCGs in each field. This leads to ~ 0.2 mag differences in E(V-I), A_V and A_I for the very red RCGs, with V-I>4 mag, corresponding to $E(V-I)\sim 3$, $A_V\sim 5.9$ and $A_I=2.9$ mag in our extinction maps. These differences are the upper limits because the atmospheric absorption in the range 900-990 nm makes the OGLE-II I-band filter closer to the standard one (Udalski et al. 2002). To make a more accurate estimate of the required correction it is necessary to have very red standard stars, with (V-I)>2.

The extinction corrected *I*-band magnitude of RCGs, $I_{0,RC}^* = 14.6$ in Baade's window is fainter than expected. Adopting distance modulus to the GC of 14.52 ± 0.1 mag (Eisenhauer et al. 2003), and assuming that the population of RCG stars in the Galactic bulge is the same as local, i.e. that the absolute magnitude is $M_{I_{0,RC}} = -0.26 \pm 0.03$ (Alves et al. 2002) and the average colour is $(V - I)_0 =$ 1.01 ± 0.08 (Paczyński & Stanek 1998), then the expected magnitude of RCG in Baade's Window should be $I_{0,RC} =$ 14.3. In Fig. 15 we show CMD and RCG centroids of BUL_SC1 (at Baade's window) before (left panel) and after (right panel) the extinction and reddening correction, with the expected RCG centroid. Note, that the difference between the average distance modulus in Baade's Window and the Galactic center is only 0.02 mag, i.e. it is of no consequence (Paczyński & Stanek 1998).

We do not know what is the solution of this problem. It may be that the population effects are large $M_{I_{0,RC}}=-0.4\sim-0.03$, as claimed by Salaris et al. (2003) and Percival & Salaris (2003), it may be that the distance to the GC is larger, or it is possible that the reddening is more complicated. We assumed that the extinction to reddening ratio is constant all the way to zero extinction. OGLE photometry is well calibrated with standards for (V-I)<2. The slope of the reddening line in Baade's Window (Region D) is well

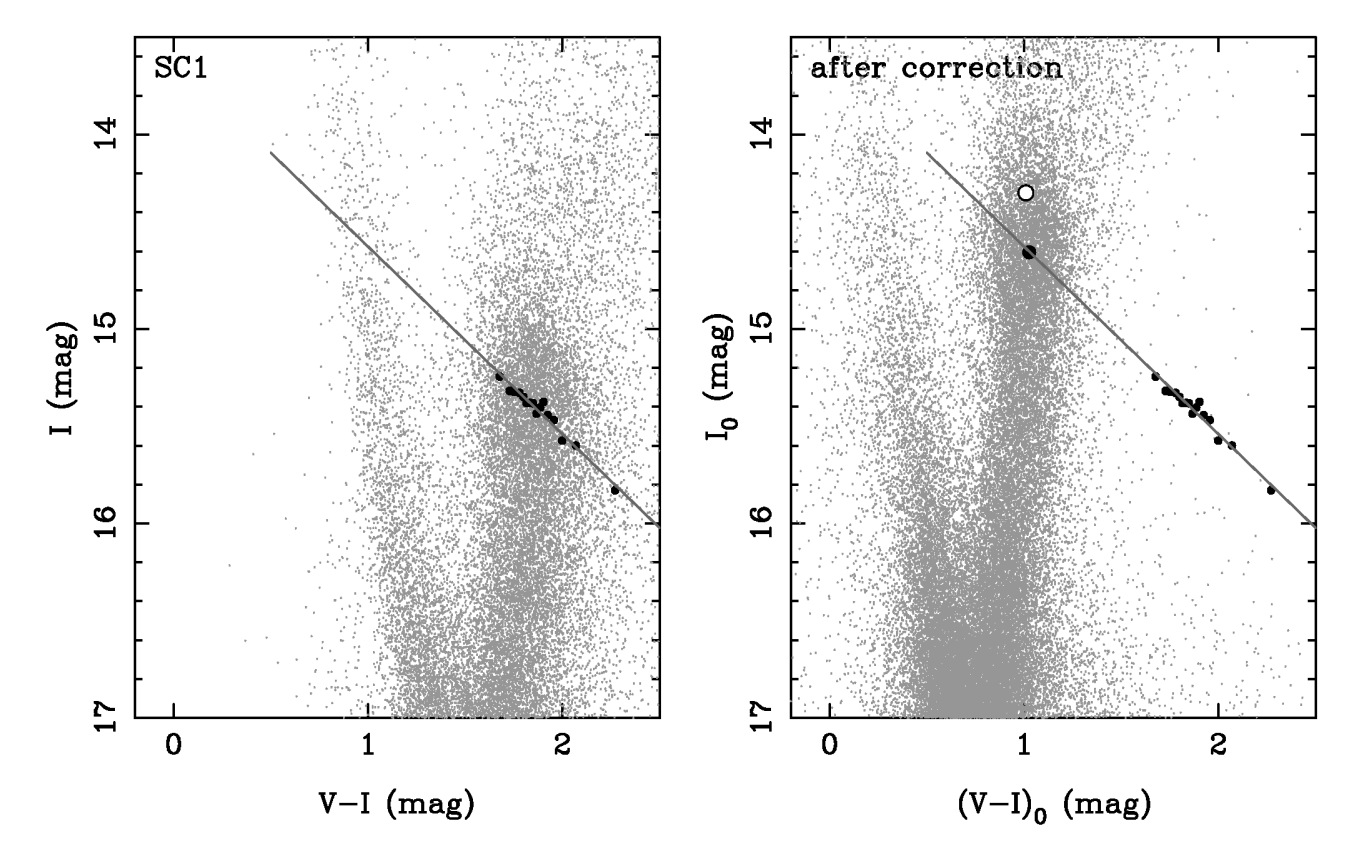


Figure 15. Colour Magnitude Diagram of BUL_SC1 before (left panel) and after (right panel) the extinction and reddening correction. Small and large filled circles indicate the same plots as Fig. 2 and RCGs centroid after the extinction and reddening correction. Open circle represents the RCGs centroid expected from the assumption that the population of RCGs in GB is the same as local. The solid line indicate the reddening line given by Eq. 3 with the mean slope $R_I = 0.964$ and a constant $I_{0,RC} = 14.6$ for this field.

measured for RCG in the colour range 1.6 < (V-I) < 2.2, but we have no direct information about the reddening line for 1.0 < (V-I) < 1.6, i.e. for the reddening range $0 < E_{V-I} < 0.6$. If we make an ad hoc assumption that the RCG population in Baade's Window is the same as local, and the distance is 8 kpc, then we may obtain $I_{0,RC}^* = 14.3$ and $(V-I)_{0,RC} = 1.0$ adopting $R_{VI} \sim 2.8$ (i.e. $R_I \sim 1.8$)for the unobserved range $0 < E_{V-I} < 0.6$. We do not know if this is plausible or not.

The situation will improve somewhat once detailed V-band OGLE photometry becomes available for RR Lyrae stars, and this will make it possible to obtain an independent estimate of the reddening in Baade's Window. Preliminary analysis of the average photometry of RR Lyrae stars seems to indicate that the puzzling brightness of red clump giants may be due to population effects, i.e. their average absolute magnitude in the Bulge is somewhat different than it is near the Sun. A much improved analysis will be done when OGLE-II V-band measurements become available in the next several months. At this time it should be OK to use our maps of differential reddening, but we consider our calibration of zero point to be uncertain. This implies that at this time our reddening maps are not adequate for a quantitative study of Galactic bar structure.

In this work we leave our extinction maps in the OGLE-II I-band because the reddening map is urgently needed for various applications, and is already used in some works

(Sumi et al. 2003b; Wray, Eyer & Paczyński 2003). A reader must take care of possible small error mentioned above while using our maps for standard I-band photometry.

The extinction map is available in electronic format via anonymous ftp from the server ftp://ftp.astrouw.edu.pl/ogle/ogle2/extinction/ and ftp://bulge.princeton.edu/ogle/ogle2/extinction/.

These extinction maps of OGLE-II GB fields facilitate the study of the Galactic structure with OGLE proper motion catalogue (Sumi et al. 2003b) and microlensing optical depth, and a study of variable stars, but the reader should be aware of the zero point of the extinction may not be accurate. We intend to improve the quality of the zero points in all fields as soon as individual OGLE V-band measurements of the RR Lyrae stars become available.

ACKNOWLEDGMENTS

We are grateful to B. Paczyński for helpful comments and discussions. We would like to thank A. Udalski for important suggestions. We acknowledge B. Drain, D. Schlegel and D. Finkbeiner for carefully reading the manuscript and comments. T.S. acknowledge the financial support from the JSPS. This work was partly supported with the following grants to B. Paczyński: NSF grant AST-0204908, and NASA grant NAG5-12212.

REFERENCES

Afonso, C. et al. 2003, A&A in press, preprint (astro-ph/0303100)

Alard, C. 1996, ApJ, 458, L17

Alcock, C. et al. 1997, ApJ, 486, 697

Alcock, C. et al. 1998a, ApJ, 492, 190

Alcock, C. et al. 1998b, ApJ, 494, 396

Alcock, C. et al. 2000a, ApJ, 541, 734

Alves, D. R. et al. 2003, ApJ, 573, L51

Bond, I. A. et al. 2001, MNRAS, 327, 868

Cardelli, J. A., Clayton, G. C. & Mathis, J. S., 1989, ApJ, 345, 245

Derue, F. et al. 1999, A&A, 351, 87

Dutra, C. M., Santiago, B. X., Bica, E. L. D. and Barbuy, B. 2003, MNRAS, 338, 253

Eisenhauer, F. et al. 2003, preprint (astroph/0306220)

Fitzpatrick, E. L. 1999, PASP, 111, 63

Gould, A. 1996, PASP, 108, 465

Gould, A., Popowski, P. & Terndrup, D. M. 1998, ApJ, 492, 778

Jones, R. V., Carney, B. W., Storm, J. & Latham, D. 1992, ApJ, 386, 646

Bono, G. & Stellingwerf, R. F. 1994, ApJ, 93, S233

Kiraga, M., Paczyński, B. & Stanek, K. Z., 1997, ApJ, 485, 611

Kurucz, R. L. 1992, IAU Symp. 149, The Stellar Populations of Galaxies, ed.B.Barbuy & A. Renzini (New York:Springer), 225

Ng, Y. K., et al. 1996, A&A, 310, 771

Nemec, J. M., Nemec, A. F. L. & Lutz, T. E. 1994, AJ, 108, 222

Paczyński, B. 1996, ARA&A, 34, 419

Paczyński, B. & Stanek, K. Z. 1998, ApJ, 494, L219

Paczyński, B. et al., 1999, Acta. Astron., 49, 319

Percival, S. M. & Salaris, M. 2003, MNRAS, 343, 539

Popowski, P. 2000, ApJ, 528, L9

Popowski, P. et al. 2003, Invited Review, to appear in "Gravitational Lensing: A Unique Tool For Cosmology", Aussois 2003, eds. D. Valls-Gabaud & J.-P. Kneib (astro-ph/0304464)

Popowski, P., Cook, K., Becker, B. 2003, AJ, in press

Salaris, M., Percival, S., Brocato, E., Raimondo, G., Walker, A. R., 2003 ApJ, 588, 801

Schlegel, D. J., Finkbeiner, D. P. & Davis, M. 1998, ApJ, 500, 525

Schultheis, M. et al. 1999, A&A, 349, L69

Stanek, K. Z. 1996, ApJ, 460, 37L

Stanek, K. Z. et al. 1997, ApJ, 477, 163

Stanek, K. Z. et al. 2000, Acta Astronomica, 50, 191

Stellingwerf, R. F. 1978, ApJ, 224,953

Stutz, A., Popowski, P. & Gould, A. 1999, ApJ, 521, 206

Sumi, T., Eyer, L & Woźniak, P. R. 2003, MNRAS , 340, $1346\,$

Sumi, T. et al. 2003a, ApJ, 591, 204

Sumi, T. et al. 2003b, preprint (astro-ph/0305315)

Udalski, A. et al. 1994, Acta Astronomica, 44, 165

Udalski, A. et al. 2000, Acta Astronomica, 50, 1

Udalski, A. et al. 2002, Acta Astronomica, 52, 217

Udalski, A. 2003, ApJ, 590, 284

Udalski, A., Kubiak, M., & Szymański, M. 1997, Acta Astronomica, 74, 319

Wray, J. J., Eyer, L. & Paczyński, B. 2003, preprint (astro-ph/0310578)

Woźniak, P. R., et al. 2001, Acta Astronomica, 51, 175 Woźniak, P. R. & Stanek, K. Z. 1996, ApJ, 464, 233